JOURNAL GEOLOGICAL SOCIETY OF INDIA
Vol.80, July 2012, pp.5-38

Petrology, Geochemistry and Fluid Inclusion Studies of Cu-Au Mineralization in Paleoproterozoic Salumber-Ghatol Belt, Aravalli Supergroup, Rajasthan

FAREEDUDDIN[1], I. R. KIRMANI[2] and SURESH CHANDER[3]
Geological Survey of India
[1]PPOD Division, SR, 40th Cross Eshwar Nagar, Bangalore - 560 082
[2]Western Region, Jhalana Dungari, Jaipur- 302 004; [3]AMSE Wing, West Zone, Jhanalana Dungari, Jaipur – 302004
Email: fareedromani@hotmail.com

Abstract: The Salumber-Ghatol belt in Rajasthan, India, situated along southern margin of the Aravalli Craton, hosts a cluster of Cu-Au deposits in calcitic and dolomitic marbles that belong to Debari Group of the Paleo-mesoproterozoic Aravalli Supergroup. The Fe-Mn rich dolomitic marble of the Delwara Formation hosts Cu-Au-Fe-oxide mineralization at Ghagri and associated distal K-Fe-Mg rich altered rocks (cryptocrystalline microcline + magnesioriebeckite + magnetite + phlogopite) and proximal feldspathised carbonate rocks (medium grained albite + microcline + dolomite + magnetite). The calcitic marble of Mukandpura Formation hosts Dugocha Cu-Au deposit with development of distal graphite-tourmaline-bearing albitites and proximal albite-microcline-magnetite rocks. Calcite and dolomite carbonates of Bhukia region with development of albite-actinolite-bearing alteration assemblages host the largest of the Cu-Au deposits in this belt. The second generation folds and associated ductile-brittle shear zones of the multiply deformed events constitute conduits for the mineralizing fluids at all locations in this belt.

Carbon isotope data for the dolomitic marbles of Ghagri area suggest mixed isotopic signatures: (i) normal marine values close to zero per mil (mean= -0.269 ‰) and (ii) enriched positive values (mean= + 4.04 ‰) akin to the 1.9 Ga global event of positive excursion. The calcitic marbles of Dugocha area have significantly depleted $\delta^{13}C$ values that are interpreted to be the result of pervasive inter-mixing of isotopically distinct carbon derived from primary depositional carbonates, hydrothermally exchanged carbonates, with significant influence of the organic carbon. The petrographic distinction of calcitic and dolomitic marbles of Bhukia area is corroborated by $\delta^{13}C$ values that show a bimodal distribution of near 0 per mil and depleted values of -3 per mil. Fluid inclusion studies suggest predominance of saline brines in the ore fluids. The $\delta^{34}S$ values for all the three deposits are narrowly constrained between 10.4 and 15.1 ‰, which suggests a common metasedimentary source for sulfur.

Identical chondrite-normalized REE patterns and primitive mantle-normalized multi-element patterns suggest a common Na- and/or K- source for the formation of Ghagri and Dugocha-Bhukia feldspathic rocks. Based on mineralization styles and attendant alteration patterns, it is argued that the mineral deposits of Salumber-Ghatol belt in the Aravalli Supergroup (i) represent sedimentary carbonate-hosted Cu-Au deposits belonging to the wider class of Proterozoic Iron-Ore-copper-Gold type (IOCG-like) mineral deposits; (ii) the fluids responsible for the mineralization are generated from common sub-crustal source and (iii) during mineralization, the influx of Na-K-rich fluids is so intense that it created 'artificial' hyper-saline conditions in the normal depositional basin that facilitated crystallization of scapolite, brucite, spadaite, povondraite and phlogopite bearing mineral assemblage.

Keywords: Petrology, Carbonates, Copper, Gold, IOCG, Mineralization, Stable Isotopes, Salumber, Ghatol, Aravalli Supergroup, Paleoproterozoic, Rajasthan.

INTRODUCTION

The Aravalli Craton in western Indian shield is a repository of several base and precious metal deposits. Among these the 4-6 km wide and 70 km long Salumber-Ghatol belt hosts over a dozen Cu-Au prospects/deposits that are currently being intensely explored by government and private agencies. The most important among the Salumber-Ghatol deposits is the Bhukia deposit located in the southern part of the belt that has emerged as the most promising gold deposit in the state of Rajasthan. Almost all

these deposits occur in calcitic and dolomitic marbles that belong to Debari Group of the Paleo-mesoproterozoic Aravalli Supergroup. Occurrence of sodic feldspathic rocks and their spatial association with mineralization is well documented in this region and these rocks are variably described in literature as quartz-feldspar rock, keratophyres, albitites, and metaexhalites (Ghariya et al. 2001; Golani et al. 2002; Guha, 2004; Rao et al. 2004). These rocks are characterized by: (i) occurrence as concordant sheets within dolomitic marbles; (ii) ambiguity of contact relationship between the host dolomites and feldspathic units, sometimes sharp without notable contact metasomatic effects and also diffuse and (iii) recrystallization of constituent minerals under low grade green schist facies of metamorphism.

In this communication we present (i) a comprehensive field and petrographic account of the three Cu-Au deposits at Ghagri, Dugocha, and Bhukia areas; (ii) report new geochemical data for the host rocks and the mineralized zones; (iii) two extreme cases of alkali-element alteration viz: ultrapotassic and ultrasodic alteration, hosted in dolomitic and calcitic marbles at two stratigraphic levels; (iv) arguments in favor of considering the Cu-Au mineralization in Salumber-Ghatol sector as similar to the IOCG-type mineralization; and (v) discuss the nature and source of the alkaline brines that converted the normal sedimentary basin into the evaporite-type basin.

GEOLOGIC SETTING

Aravalli craton is a composite of several major tectonic units of Precambrian age (Fig. 1). These include: (1) ≈ 3.0 Ga old terrain of polyphase granitoids (tonalite, trondhjemite and granites), gneisses with enclaves of amphibolites and metasediments and linear supracrustal belts having greenstone-like affinities of Archaean ancestry collectively named as the Banded Gneiss Complex (BGC, Heron, 1953); (2) Paleo- to Mesoproterozoic Ajmer Formation composed of calcareous and pelitic sediments; (3) Paleo- to Mesoproterozoic Aravalli Supergroup; (4) Meso- to Neoproterozoic Delhi Supergroup, exposed in the axial regions of the Aravalli mountain range; predominantly composed of tectonised metavolcanics and metasediments presumably of ophiolitic lineage; (5) ~ 1 Ga old Punagarh supracrustal belts of rift-related origin, (6) younger (~ 850 Ma old) Erinpura type granitoid rocks and (7) Neoproterozoic (~ 750 Ma old) anorogenic Malani magmatic suite.

The Aravalli Supergroup, the focus of the current study, is exposed in the southern and southeastern parts of the Aravalli craton and represents a volcano-sedimentary accumulation in a shelf-like environment (Roy, 1988) which unconformably overlies the gneisses of BGC and is composed of a mafic volcanic sequence in the basal

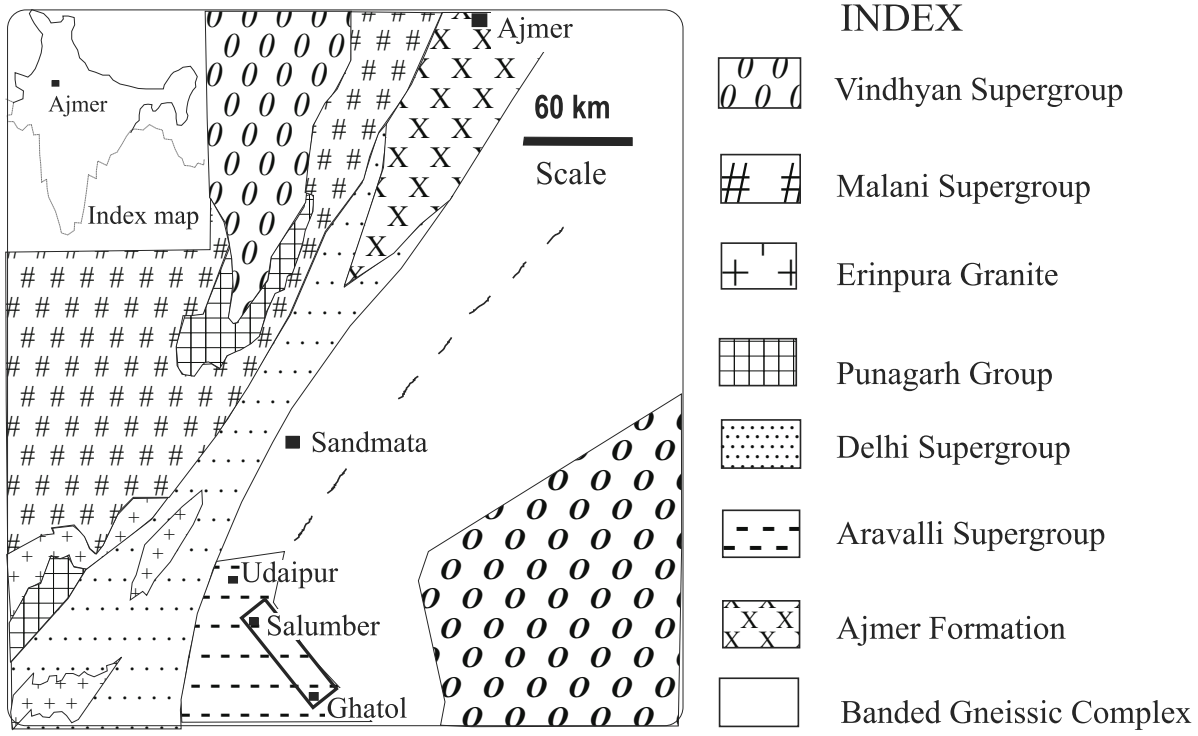

Fig.1. Regional geological map of Rajasthan (simplified from Gupta et al. 1997; Ajmer Formation shown after Fareeduddin et al. 1995).

stratigraphic units that gives way to predominantly calcareous and argillaceous sediments higher up in the stratigraphy. Its stratigraphic order, as outlined by two major research groups (Roy, 1988; Gupta et al. 1997) has conflicting interpretations that relates to intricacies of internal organization of the major lithologic markers owing to a complex structural pattern. Notwithstanding the differences both the groups broadly recognize three major events in the development of the Aravalli basin: (i) outpouring of mafic/ultramafic lavas during the initial development of the Aravalli basin (Delwara volcanic rocks in the Debari Group); (ii) extensive development of platformal sedimentary sequences during the main basin formation event (Jaisamand, Berwas-Mukandpura, and Jhamarkotra-Jagpura Formations of Debari Group) and (iii) deepening of the Aravalli basin and development of deep-sea sedimentary facies towards the west (Jharol Group).

The Aravalli supracrustals have undergone three main phases of folding (Naha and Halyburton, 1974). The first generation folds are reclined or inclined with dominantly easterly or westerly plunge; the second phase folds have steep inclined axial planes with variable fold geometry from isoclinal to open folds. The third phase folds are generally in the form of broad warps with EW or WNW-ESE striking sub-vertical axial planes and invariably refold the earlier folds. The supracrustals are recrystallized under regional green schist facies conditions with few local areas recording middle amphibolite facies assemblages (Sharma, 1988).

The basal Delwara volcanic rocks are LREE-enriched komatite, komatiitic tholeiites, picritic basalts, and tholeitic basalts formed from a number of mantle sources, as well as different degrees of melting (Ahmed and Rajamani, 1991).

Geology of the Cu-Au Deposits in Salumber Ghatol Sector

The regional geological map of the Salumber-Bhukia-Ghatol areas is presented in Fig.2A. This area is located about 130 km ESE of Udaipur and presumably represents the southeastern extension of the litho-units exposed in the type-section in Udaipur-Debari sector (Roy, 1988). The Lower Debari Group (Table 1) in the area includes the Gurali Formation (quartzite/conglomerate that directly overlies BGC), and the Delwara (mainly metabasaltic rocks), and Jaisamand Formations (mainly conglomerates/quartzite). The Upper Debari Group is extensive in this region and is represented by the Mukandpura and Jagpura Formations. The Mukandpura Formation is characterized by dolomites, phyllites and carbonaceous phyllites with intercalations of mica schist. The Jagpura Formation consists of meta-pelites (mainly quartz-mica schist and garnet-biotite schist) and dolomitic marble.

The Ghagri area, situated about 15 km east of Salumber, exposes rocks belonging to the Delwara Formation (Fig. 2B). A thick polymictic conglomerate represents a clear-cut unconformity between the Archaean basement and these Paleoproterozoic supracrustal rocks. The other Delwara units exposed in this area include mafic metavolcanics, dolomite, carbonaceous phyllite, chlorite schist, and quartzite. The mafic metavolcanics and dolomite overlie the basal conglomeratic units and the dolomite in turn is overlain by carbonaceous phyllite, chloritic phyllite, calc-biotite schist with intercalations of milky white quartzite. The dolomite is inter-layered with thin bands of grey feldspathic rocks and quartzite and typically shows brecciated features with angular fragments of chert and quartzites.

The Dugocha area lies about 40 km southeast of Salumber and exposes dolomites, schistose and massive metavolcanic rocks, graphitic albite-tourmaline rock and calc silicates belonging to the Jagpura Formation of the Debari Group (Fig. 2C). A thin band of calc-silicate occurs on either side of graphitic albite-tourmaline rock. A linear band of quartz-mica schist with graphite occurs to the northwest of calc silicate rock. The mica schist consists of muscovite as

Table 1. Aravalli stratigraphy of the Salumber-Ghatol belt and its comparison with Debari Sector (*after* Gupta et al. 1997)

	Debari Sector		Salumber-Gharol Sector	
Debari Group	Jhamarkotra Formation	Quartzite dolomite phosphatic limestone	Jagpura Formation	Quartzites, schist, garnet-mica schist dolomites
	Berwas Formation	Quartzites, phyllites, carbon phyllites dolomites	Mukundpura Formation	Carbon phyllites dolomites
	Jaisamand Formation	Conglomerates, quartzites, phyllites	Jaisamand formation	Conglomerates, mica schist
	Delwara Formation	Mafic Volcanics, marble schist, phyllites quartzites	Delwara Formation	Mafic Volcanics, marble quartzites
	Gurali Formation	Quartzites	Gurali Formation	Quartzites

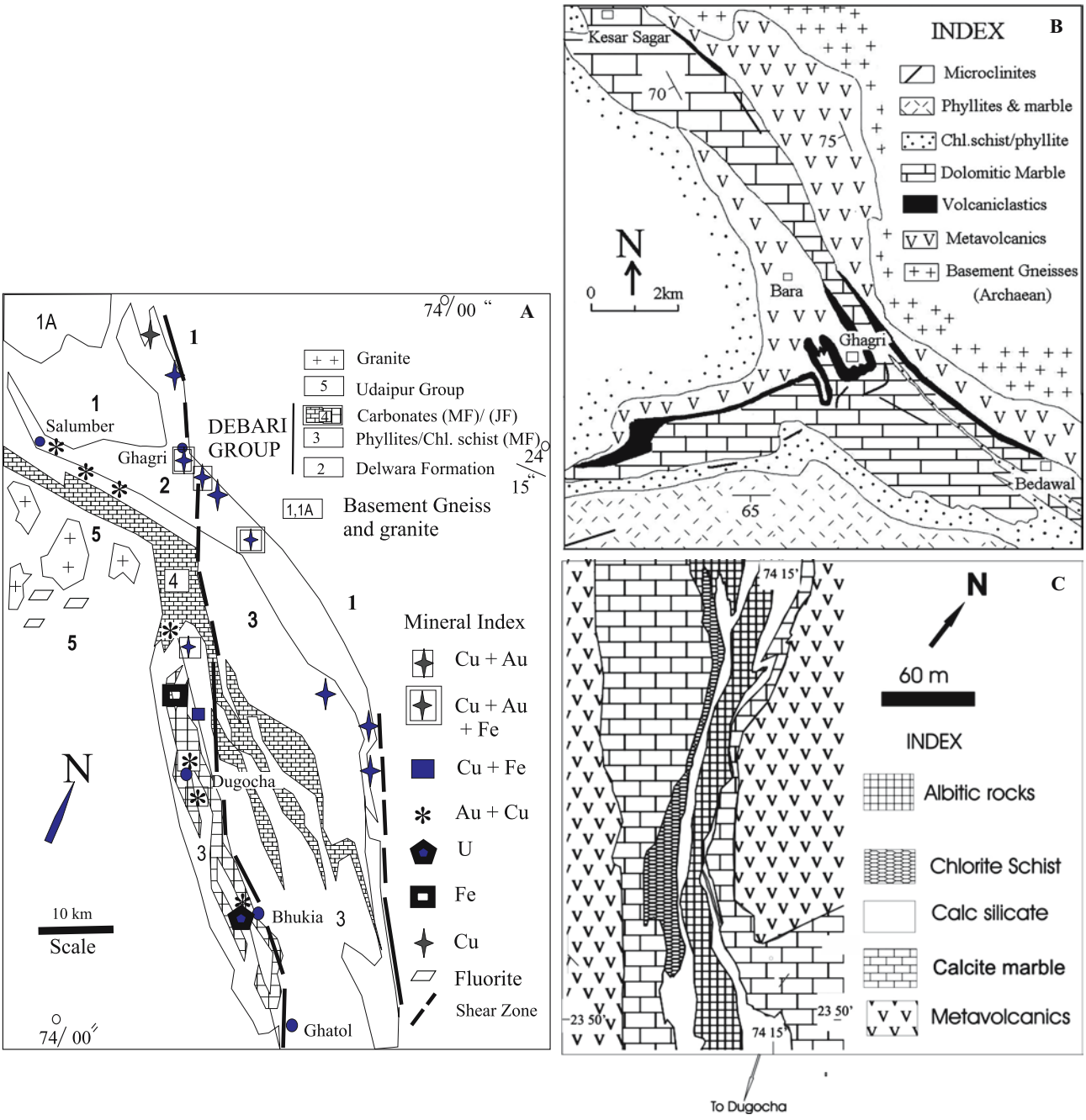

Fig.2. (A) Geological and mineral map of Salumber-Ghatol belt showing mineral prospects/deposits of Cu + Au, Cu + Au + Fe, Cu + Fe, Au + Cu, U, Fe and fluorite. **(B)** Geological map of Ghagri area. **(C)** Geological map of Dugocha Cu-Au prospect.

the predominant mineral with minor biotite and sericitised alkali feldspar. Quartz occurs both as granoblastic aggregates and also as stretched ribbons. Coarse-grained, stretched graphite flakes occur parallel to the foliation in the rock.

In Bhukia area (Fig 2D) the metasedimentary units of the Debari Group tectonically overlie the basement crystallines along NNW-SSE trending Ghatol thrust. The rock types along the thrust contact exhibit steep dip towards southwest, extensive retrogressive metamorphic assemblages, development of S-C fabric and extensive silicification. The Bhukia deposit and associated prospects occur in the major dolomitic marble band that constitutes the uppermost marble unit of Debari Group in this region. The dolomitic marble unit occurs as parallel bands of varying thicknesses within the phyllite, carbonaceous phyllite, and chlorite schist unit (Fig.2D). The dolomitic marble grades

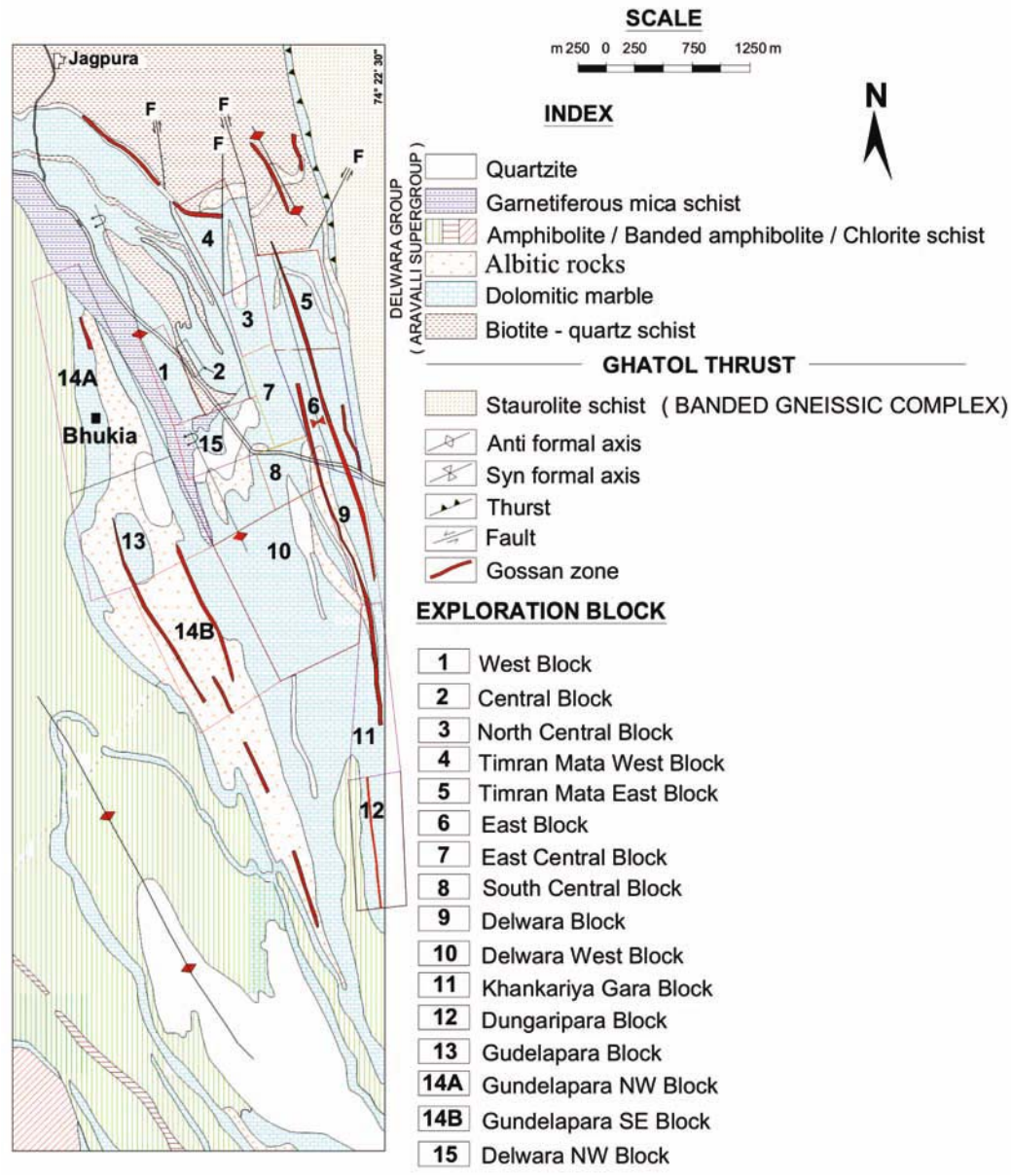

Fig.2D. Geological map of Bhukia area (*after* GSI, 2009).

imperceptibly to calcite-bearing dolomitic marble, calc silicates and amphibole-rich marble. Oxide minerals (hematite, maghemite) and rare titanites, tourmaline and apatite occur as minor minerals. The amphibole-bearing units have actinolite, tremolite, and diopside as ubiquitous minerals besides the carbonate minerals. The dolomitic marbles contain (i) fairly thick intercalations of quartz-chlorite schist, (ii) interbands of quartzites, and (iii) feldspathic and quartzo-feldspathic rocks. The latter two units constitute well-defined markers in the area.

There are four small to medium size granite plutons, collectively referred as Jhalara granites, occuring towards northwestern part of the Salumber-Ghatol belt. These intrude chlorite schist and phyllites of Udaipur Group. The eastern contact of the Jhalara granite with the Aravalli sequence is sheared with intensely comminuted rock fragments dominating the contact region. Two variants of granites could be recognized in field. These are (i) grey non-porphyritic, crudely foliated granites and (ii) pink porphyritic granites. The contact relationship between the two variants is ambiguous, as at some places cross cutting relationship of the pink porphyritic variant into the grey granites noticed but at majority of the places the contacts relationship is diffused. The grey granite is essentially made up of quartz, plagioclase, microcline and biotite. The pink granites possess fractured phenocrysts of pink albite that range in size from

few mm up to 6 cm in a groundmass of albite, microcline, minor biotite and quartz. The pink granite phase is intruded by veins of pink albitites, calcite-albite veins, quartz-calcite veins, calcite-fluorite veins and calcite-fluorite-speccular hematite veins. In proximity of the granites, the host phyllites are intensely traversed by albite veins with fluorite and specular hematites. These were prospected for fluorite mineralization but found to be uneconomical (Gupta et al. 1997).

The entire sequence in Salumber-Ghatol belt has undergone polyphase deformation. Small-scale isoclinal to tight folds with attendant schistosity (S1) represent the first phase of folding. The latter are refolded on NNW-SSE trending, subvertical second generation structures. The major lithological markers of the region, particularly in Ghagri and Bhukia area, exhibit regional-scale fold patterns. The second generation folds are also associated with subvertical ductile to ductile-brittle shear zones. Open style cross folds represent the third phase of folding in this area. A single metamorphic recrystallization event under green schist facies regional metamorphism and a pervasive post-tectonic hydrothermal activity resulting in several mineral deposits in structurally favorable loci characterizes the Salumber Ghatol belt.

ANALYTICAL TECHNIQUES

Whole-rock analyses was carried out using Phillip's X-UNIQUE X-ray Spectrometer. Some mineral phases were identified by using PAN Analytical X'PERT PRO XRD System. The trace-element, including rare earth-element analyses was carried out by Inductively Coupled Plasma-Mass Spectrometry (ICP-MS) and Instrumental Neutron Activation Analyses (INAA) methods. The sulfur isotopic work on sulfide separates was carried out using Nuclide 6-60 Gas Source Ratio Measurement Mass Spectrometer. The Carbon and Oxygen isotopic studies on host carbonates and graphite from the alteration zones were carried out in the dual inlet mode of Sercon Geo 20:20 Isotope Ratio Mass Spectrometer using the CAPS peripheral unit following on-line extraction of CO_2. The mineral analyses of the silicate and ore minerals from different rocks and ores were carried out by using CAMECA SX-100 electron microprobe. The microthermometric studies on fluid inclusions from the ore zones were carried out on a Linkam THMS 600 heating/freezing stage fitted on a Olympus BX 50 transmitted light microscope. The instruments X-UNIQUE X-ray Spectrometer, PAN Analytical X'PERT PRO XRD System, Nuclide 6-60 Gas Source Ratio Measurement Mass Spectrometer, Sercon Geo 20:20 Isotope Ratio Mass Spectrometer and Linkam THMS 600 heating/freezing stage fitted on a Olympus BX 50 transmitted light microscope are located at the Petrology, Petrochemistry and Ore-Dressing (PPOD) laboratory, RSAS Wing of the Geological Survey of India (GSI), Bangalore. The ICP-MS unit is located at the Chemical Division of GSI, Hyderabad and INAA at Chemical Laboratory, GSI, Pune. The CAMECA SX-100 microprobe is located at EPMA Laboratory, Central Petrological Laboratory, GSI, Kolkata. Details of sample preparation and the analytical procedures adopted and the standards used for each of the above analytical techniques are available with the author and would be supplied on request.

CARBONATE ROCKS

Dolomites of Ghagri area

Geology and Petrography: Dolomite, most extensive of the lithological units of the basal Aravalli sequence of Delwara Formation in Debari Group, is traceable for over forty kilometers from Salumber in the west to Morela in the east and further extending south of Bedawal (Fig. 2B). The carbonate is steel grey to greyish brown in color, fine-grained and locally carbonaceous (graphitic) in nature with occasional disseminations of pinkish tabular albite. The rock contains 90% of dolomite, with minor amount of euhedral albite and accessory amounts of mica and chlorite. The carbonate bands proximal to the mineralized zones, designated in this study as mineralized carbonates are brownish and pinkish colored, exhibit medium- to coarse-grained, granoblastic textures and contain fractured and deformed dolomite, tourmaline, biotite, and sulfide minerals. The carbonate minerals show incipient lamellar twinning (presumably an early effect of albitisation of carbonates) and biotites are altered to non-pleochroic bleached flakes. Mineral chemistry (Table 2) suggests that (i) the carbonate mineral in both types of carbonate rocks is dolomite with no significant chemical variation between them with the exception of the dolomite grains in mineralized carbonates which are significantly richer in iron ($Fe_2O_3^T$ = 0.97 wt % to 5.82 wt %) and manganese (MnO = 0.51 to 2.12 wt %); (ii) micas are richer in MgO (at times phlogopitic); and (iii) tourmaline is dravitic in composition.

Geochemistry: Both normal and mineralized dolomites possess near identical whole-rock major element geochemical composition (Table 3) being reflected in higher iron ($Fe_2O_3^T$ = 5.20 to 8.43 wt %) and manganese (MnO = 0.47 to 2.35). However, the chemical difference between these two types of carbonates could be seen in their REE

Table 2. Representative Chemistry of Minerals from carbonate rocks of Ghagri and Dugocha areas

	Ghagri Area Carbonates												Dugocha Area Carbonates			
	Dolomites					Mineralized Carbonates				Mica	Chl	Tour	Calcite			Tour
	1	2	3	4	5	6	7	8	9	10	11	12	13	14	15	16
SiO_2	0	0	0.01	0	0.02	0	0.04	0	0	36.69	28.37	37.78	0.04	0.01	0.06	36.98
TiO_2	0	0.05	0.02	0	0	0	0	0.07	0	1.97	0.1	0.2	0	0.06	0	1.62
Al_2O_3	0	0	0.02	0	0	0	0.03	0	0	13.75	17.91	31.13	0	0.04	0	27.62
Fe_2O_3	0.97	1.06	0.91	4.32	1.02	1.06	5.66	5.82	5.58	17.07	16.61	5.25	0.12	0.04	1.29	2.36
MnO	0.69	0.51	0.61	2.12	0.59	0.62	2.15	1.95	2.05	0.1	0.21	0.01	0.08	0	0.16	0.09
MgO	21.89	21.03	21.66	18.56	21.2	22.37	17.89	17.79	17.4	14.18	22.21	9.89	0	0.28	0	12.49
CaO	31.88	32.43	30.83	30	29.27	31.6	29.66	28.78	29.39	0.01	0.02	0.17	54.2	56.72	57.23	3.35
Na_2O	0	0.01	0	0.04	0.01	0.02	0.02	0.05	0.04	0.09	0.05	2.96	0.51	0.03	0.03	1.28
K_2O	0	0	0	0	0.04	0	0	0	0.01	8.99	0.05	0	0.1	0.04	0	0.08
P_2O_5	0.26	0.27	0.24	0.21	0.29	0.27	0.25	0.22	0.25	0	0.03	0.04	0.07	0	0	0.00
Cr_2O_3	0.06	0	0	0	0.03	0	0	0	0	0	0	0	0.02	0.04	0.12	0.00
BaO	0.17	0	0	0	0	0	0	0	0.14	0.03	0.06	0	0	0.06	0	0.00
Total	**55.92**	**55.36**	**54.3**	**55.25**	**52.47**	**55.94**	**55.7**	**54.68**	**54.86**	**92.88**	**85.62**	**87.43**	**55.14**	**57.32**	**58.89**	**85.87**

Abbreviations: Chl = Chlorite, Tour = Tourmaline

abundances. Whereas the ΣREE (Table 3) for the normal carbonates is very low (38 and 27 ppm), it is higher for the mineralized carbonates (53 to 73 ppm). The shale-normalized REE pattern (Fig.3) for the normal carbonate shows a strong negative cerium (Ce) anomaly (average Ce/Ce* = 0.78) suggesting marine depositional environment. The mineralized carbonates display subtle negative Ce anomaly (average Ce/Ce* = 0.91), but significantly enriched middle rare earth elements showing dumbbell shaped REE patterns. The latter could be attributed to the intense hydrothermal alterations (that accompany the Cu-Au mineralization) of the normal marine carbonates.

C-O Isotopes: $\delta^{18}O_{PDB}$ and $\delta^{13}C_{PDB}$ values for non-mineralized and mineralized carbonates are given in Table 4. The subtle difference in major and trace elements of these two carbonates (Table 3) is also reflected in their stable isotopic signatures. The average $\delta^{18}O_{(SMOW)}$ values for normal and mineralized dolomites are 16.58 per mil and 20.53 per mil, respectively and are comparable to the average marine carbonates of Paleoproterozoic age (Shields and Veizer, 2002). The C isotopic data ($\delta^{13}C_{PDB}$) exhibits two distinct signatures for non-mineralized carbonates viz: (i) normal marine signature close to zero per mil (mean = -0.27 ‰) and (iii) enriched positive values (mean = + 4.04 ‰). The $\delta^{13}C_{PDB}$ values for mineralized carbonates are much depleted (mean = -4.46 ‰). Results of several studies have documented that the depositional C-isotopic values are generally preserved in whole-rock samples of carbonate except in cases where (i) re-equilibration of existing C-isotopic values occur with influx and interaction of fluids of different isotopic composition, (ii) de-carbonic alterations in presence of siliciclastic rocks, and (iii) oxidation of organic matter during precipitation of marine carbonates (Fairchild et al. 1990; Kaufmann et al. 1992). The preponderance of the $\delta^{13}C_{PDB}$ values close to 0 per mil in Ghagri carbonates attest to their normal marine depositional environment, but depletion and enrichment of the values, respectively, in mineralized and non-mineralized carbonates suggest two distinctly different post-depositional events that the carbonates of this area have witnessed. The samples that record depleted values contain disseminations of albitic feldspar, exhibit silica and soda enrichment and show REE patterns that are distinctly different from the patterns of normal marine carbonates affected by the hydrothermal alteration. The depleted values are proximal to the diagenetic trend and far away from the field of primary carbonates (Fig. 4, Burdett et al. 1990). The depleted $\delta^{13}C_{PDB}$ in these carbonates therefore may reflect an event of decarbonation during the albitization of carbonates. The strong positive values in excess of + 5 per mil in non-mineralized carbonates on the other hand, apparently correspond to a global event of positive excursion during 1.9 Ga year period. The values recorded from the Ghagri carbonates are closer to the reported positive excursion values of $\delta^{13}C_{PDB}$ + 6 to + 11 per mil from Jhamarkotra phosphatic carbonates (Sreenivas et al. 2001) that occur further north of Ghatol-Salumber belt and are stratigraphically equivalent to the Ghagri carbonates. A much more detailed analysis of this type of carbonate in evaluating evolution of Paleoproterozoic carbon-isotopic signatures is therefore warranted. An important observation from Table 4 and Fig.4 is that the $\delta^{18}O_{PDB}$ values of Ghagri carbonates are much lighter compared to the carbonates from

Table 3. Whole rock geochemistry of carbonates from Salumber-Ghatol belt

	Ghagri Carbonate		Min. Carbonates			Dugocha Carbonates			Mineralised Carbonates					Bhukia Carbonate		Min. car
	1	2	3	4	5	6	7	8	9	10	11	12	13	14	15	16
Samp.No.	1/F-SG2	SG-6	2/F-SG11a	3/F-SG11c	5/F-SG11aa	21/F-SD2	23/F-SC1	24/F-SC3	27F-SC-7	22/F-SD1	25/fF-SC5	26F-SC6	DGHW-2	Bhu-1	F-4	Bhu-2
XRF No.	22556	22559	22562	19327	22563	ER-4	ER-3	ER-5	22559	24869	22557	24872	24477	ER-1	24474	ER-2
SiO_2	6.83	10.99	5.2	5.31	6.7	2.36	3.03	8.52	3.23	4.09	5.58	6.08	4.73	2.65	2.38	5.52
TiO_2	0.26	0.07	0.09	0.06	0.09	0.01	0.02	0.1	0.32	0.03	bld	bld	bld	0.07	bld	0.1
Al_2O_3	1.69	bld	bld	0.69	bld	0.4	1.81	2.05	2.01	bld	1.03	bld	bld	0.97	bld	2.05
Fe_2O_3	5.64	5.2	8.01	8.43	7.05	1.23	1.42	2.03	1.98	1.89	2.65	3.31	24.84	3.04	21.9	3.05
MnO	0.51	0.47	2.06	2.35	2.06	0.22	0.35	0.26	0.25	0.25	0.18	0.12	1.14	0.29	1.85	0.26
MgO	14.01	18.59	14.44	15.12	15.64	1.16	0.76	1.38	0.67	1.06	1.18	1.02	bld	1.16	bld	1.58
CaO	28.54	27.55	25.5	25.21	24.65	52.86	51.87	47.97	50.78	48.2	46.66	45.35	28.82	51.86	31.99	49.95
Na_2O	2.86	0.71	0.32	0.28	0.42	0.16	0.22	0.97	0.22	0.19	0.54	0.09	bld	0.15	0.87	0.97
K_2O	0.23	0.1	0.77	0.56	0.59	0.1	<0.01	<0.01	<0.01	bld	bld	bld	bld	0.05	bld	<0.01
P_2O_5	0.1	0.13	0.06	0.13	0.06	0.03	0.03	0.12	0.03	0.13	0.24	0.35	0.27	0.09	0.13	0.12
S	0.04	0.26	0.23	0.22	0.33	nd	nd	nd	nd	1.63	0.14	0.28	2.76	0.1	1.99	nd
Cr_2O_3	bld	bld	0.23	bld	0.27	nd	nd	nd	nd	bld	bld	bld	bld	bld	bld	nd
NiO	bld	bld	bld	bld	bld	nd	nd	nd	nd	0.01	bld	0.02	0.01	bld	0.01	nd
BaO	0.02	0.03	0.03	0.01	0.03	nd	nd	nd	nd	0.11	bld	0.22	0.1	bld	0.11	nd
LOI	38.07	36.39	43.17	41.58	41.12	40.56	41.4	35.37	40.45	42	43.44	42.62	37.32	40.05	38.75	35.37
Total	**98.8**	**100.49**	**99.99**	**99.95**	**99.01**	**99.09**	**100.91**	**98.77**	**99.94**	**99.59**	**101.64**	**99.46**	**99.99**	**100.48**	**99.98**	**98.97**
Ba	10	20	10	10	10	80	85	110	75	80	70	90				
Sr	170	190	85	90	100	100	110	90	90	90	100	140				
Be	<0.3		<0.3	1.638	<0.3	<0.3	<0.3	<0.3	0.4	<0.3	<0.3	<0.3				
Ga	6.043		3.556	12.021	0.999	1.722	1.16	1.868	1.214	1.174	1.2	2.326				
Ge	1.022		<0.05	2.371	0.116	<0.05	<0.05	<0.05	<0.05	<0.05	<0.05	<0.05				
As	2.027		3.2	<2	<2	149.582	19.808	18.188	10.608	20.772	3.6	5.61				
Y	10.5347		8.4282	12.5653	16.7288	18.8078	11.0594	10.2212	28.545	17.3008	7.227	21.4016				
Zr	44.078		29.768	51.091	21.184	15.742	20.742	17.724	8.8	19.182	16.3	30.55				
Nb	5.843		4.624	5.974	0.991	3.538	3.752	3.24	1.08	5.95	4.91	3.484				
Cs	<0.2		<0.2	1.301	0.438	<0.2	<0.2	<0.2	0.28	<0.2	<0.2	<0.2				
Hf	1.275		0.758	1.348	0.485	0.426	0.486	0.598	<0.2	0.552	0.42	0.526				
Bi	<0.1		<0.1	<0.1	<0.1	0.2	0.12	0.388	<0.1	<0.1	<0.1	<0.1				
Th	2.27		0.8	2.695	0.321	0.956	0.6	30.842	<0.2	0.696	0.976	1.37				
U	0.641		<0.5	0.78	0.611	<0.5	1.292	<0.5	<0.5	<0.5	1.636	2.096				
La	6.84		4.39	15.262	12.608	17.628	9.224	69.736	1.54	2.234	6.974	7.32				
Ce	14.266		9.164	29.971	16.464	24.678	11.952	151.102	2.68	4.846	12.294	18.024				
Pr	1.761		1.138	3.234	2.601	3.546	1.71	10.672	0.308	0.668	1.402	2.492				
Nd	6.937		5.19	12.521	10.467	14.174	6.434	33.604	1.266	3.424	5.586	12.212				
Eu	0.341		0.514	0.713	0.516	0.716	0.576	0.716	0.152	0.14	0.486	0.658				
Sm	1.578		1.518	2.55	2.308	3.032	1.132	3.828	0.374	1.084	1.024	3.634				
Tb	0.268		0.248	0.373	0.361	0.476	0.184	0.392	0.218	0.288	0.152	0.656				
Gd	1.631		1.696	2.329	2.368	3.004	1.21	2.722	0.744	1.502	0.98	3.803				
Dy	1.664		1.294	2.11	2.188	2.62	1.088	1.802	2.072	1.918	0.85	3.68				
Ho	0.351		0.238	0.422	0.448	0.53	0.252	0.342	0.706	0.45	0.184	0.7				
Er	0.899		0.544	1.067	1.142	1.262	0.652	0.826	2.59	1.172	0.458	1.634				
Tm	0.155		0.08	0.171	0.167	0.19	0.092	0.136	0.542	0.188	0.074	0.256				
Yb	0.93		0.474	1.06	0.93	1.018	0.502	0.796	3.698	1.148	0.396	1.48				
Lu	0.137		0.072	0.156	0.13	0.14	0.052	0.112	0.588	0.164	0.058	0.198				
ΣREE	37.758	0	26.56	71.939	52.698	73.014	35.06	276.786	17.478	19.226	30.918	56.747				

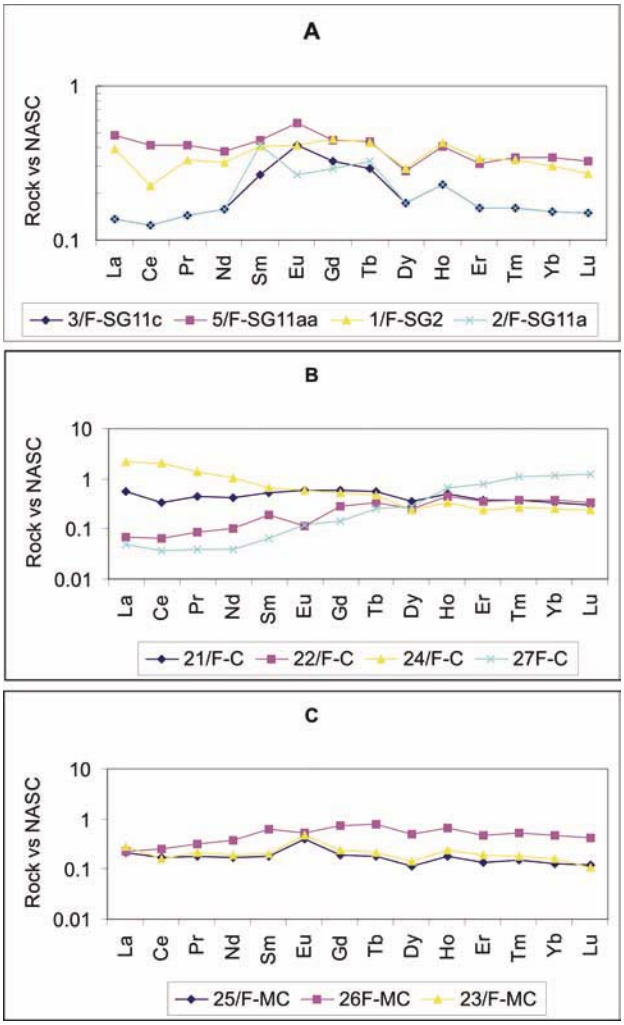

Fig. 3. Shale-normalized REE patterns for the Ghagri and Dugocha-Bhukia carbonates (normalizing values after Haskin et al. 1968). **A**. Ghagri dolomitic marbles (1/F and 5/F) and mineralized dolomitic marbles (2/F and 3/F). **B**. Carbonates from Dugocha-Bhukia areas. **C**. Mineralized calcitic marbles from Dugocha-Bhukia areas.

evaporitic environment and follows a trend distinctly different from the evaporitic trend.

Dugocha-Bhukia Carbonates

Geology and Petrography*:* An extensive sequence of carbonate rocks belonging to the upper stratigraphic horizons of the Jagpura Formation of the Debari Group occurs from north of Dugocha to the south of Bhukia. Massive to thickly bedded grey colored carbonates in Dugocha area are medium to coarse grained almost entirely made up of polycrystalline aggregates of calcite with minor amounts of albite and tremolite. The carbonates proximal to the mineralized zones are greyish brown in color and shows frequent silicification and ferruginization along ductile shear zones. Petrographically, about 90 percent of the mineralized carbonate rock is made up of a granoblastic mosaic of dusty and clouded calcite, minor amount of albitic plagioclase, quartz and accessory amounts of chlorite, graphite, biotite, sulfides and tremolite. Mineral chemistry (Table 2) in both variants of the rock shows that the carbonate is exclusively represented by calcite. The latter (analysis no.15, Table 2) possesses minor amounts of iron and traces of manganese.

The Bhukia carbonates are not as homogenous as that of carbonates of Dugocha area. They are represented by intermingled varieties of calcitic marble (calcite + albite + actinolite), dolomitic marble (dolomite + calcite + phlogopite + tourmaline + titanite), scapolite-bearing marble (scapolite + dolomite + calcite + plagioclase + tourmaline), tremolitic marble (dolomite + tremolite + phlogopite + sphene) and calc silicates (calcite + tremolite + diopside + titanite). Besides brucite is reported from these carbonates (Guha, 2004).

Geochemistry: The major-element compositions of both mineralized and non-mineralized carbonates from Dugocha area are almost identical, attesting calcitic marble character of carbonates (Table 3). The difference, however, is in the elevated abundance of Na_2O and Al_2O_3 in normal carbonates and Fe_2O_3 and sulfur in the mineralized carbonates that are due to respective presence of albite and magnetite in them. The ΣREE of the Dugocha carbonates though generally low for both the variants of carbonates (17 ppm to 56 ppm) one sample exhibits high ΣREE (277 ppm). Both non-mineralized and mineralized carbonates show negative Ce anomaly (average Ce/Ce* = 0.91 and 0.81 respectively). The most distinctive feature of the shale-normalized rare element pattern is the highly variable LREE with both negative and positive Eu anomaly (Fig. 3).

C-O Isotopes*:* The $\delta^{18}O_{PDB\ \&\ SMOW}$ and $\delta^{13}C_{PDB}$ values for non-mineralized and mineralised carbonates from Dugocha area are presented in Table 4. The$\delta^{18}O_{smow}$ data suggests that there is no perceptible difference between the mineralized (average = -15.26 ‰) and non-mineralized carbonates (average = -12.29 ‰) in the Dugocha area. These values are depleted with respect to the average marine carbonate of Paleoproterozoic age (-11 ± 3 ‰; Sheilds and Veizer, 2002). The $\delta^{13}C_{PDB}$ data for non-mineralized carbonates are of the range from -1.22 to – 6.35 per mil with an average of -4.13 ‰, which are highly depleted in comparison to the global mean $\delta^{13}C_{PDB}$ data of marine carbonates (0 ± 2 ‰, Sheilds and Veizer, 2002). The values are much closer to the values reported for the primary carbonates. The depleted $\delta^{13}C_{PDB}$ values of Dugocha

Table 4. Carbon and Oxygen isotope values in carbonates from Salumber-Ghatol Belt and Carbon isotope values of graphite of Dugocha altered rocks

Sl. no.	Sample No	Sample Description	δ^{13C} (‰) (PDB)	$\delta^{18}O$ (‰) (SMOW)	$\delta^{18}O$ (‰) (PDB)
Ghagri Area					
		Dolomites			
1	1/SG	Dolomite in finely crystaline grey carbonate	5.31	17.9	-12.622
2	8/RGH-3	Dolomite in finely crystalline grey carbonates	5.34	-19.97	-12.02
3	2/SG	Dolomite in white carbonate	1.49	13.87	-16.529
4	4/SG	Dolomite in grey Carbonate, laminated	-0.211	15.86	-14.598
5	5/SG	Dolomite in finely crystalline grey carbonates	-0.299	15.92	-14.537
6	6/SG	Dolomite in finely crystalline grey carbonates	-0.298	15.96	-14.505
		Mineralized Dolomites			
7	3/SG	Dolomite in brown carbonates with feldspar disseminations	-4.14	26.28	-4.487
8	7/SG	Dolomite in brown carbonates with feldspar disseminations	-4.773	14.78	-15.644
Dugocha Area					
		Calcite Carbonates			
9	SD-2	Calcite in white carbonate	-1.68	15.04	-17.09
10	8/SD	Calcite in greyish white carbonate	-7.087	16.02	-14.446
11	9/SD	Calcite in brown carbonate	-0.212	15.84	-14.622
12	10/SD	Calcite in greyish brown carbonate	-1.997	21.69	-8.946
13	11/SD	Calcite in grey carbonate	-4.896	14.49	-15.93
14	12/SD	Calcite in grey carbonate	-4.832	13.39	-16.474
15	16/SD	Calcite in grey carbonate	-5.9	14.49	-15.928
16	17/SD	Calcite in white carbonate	-4.908	12.32	-18.03
17	SD10-A	Calcite in white carbonate	-4.67	14.09	-15.03
18	SC-1	Calcite in white carbonate	-5.63	13.56	-16.7
19	SC-2	Calcite in white carbonate	-2.41	13.83	-16.44
20	SC-3	Calcite in white carbonate	-5.09	9.97	-20.15
21	SC-4	Calcite in white carbonate	-4.66	9.46	-20.64
22	SC-5	Calcite in white carbonate	-2.49	13.57	-16.69
23	SC-6	Calcite in white carbonate	-1.22	11.97	-18.23
24	SC-7	Calcite in white carbonate	-5.18	12.68	-17.54
25	SC-8	Calcite in white carbonate	-6.35	13.29	-16.96
		Graphitic Carbon			
26	C1	Graphite in graphitic albitites	-17.05		
27	C2	Graphite in graphitic albitites	-19.08		
Bhukia Area*					
28	BJR-1	Dolomite Marble	-1.5	21.5	
29	BJR-2	Dolomite Marble	-0.4	21.4	
30	BJR-3	Dolomite Marble	-4.1	26.8	
31	BJR-6	Dolomite Marble	-0.5	19.7	
32	BJR-8	Dolostone	-0.3	21.8	
33	BJR-9	Dolostone	-0.9	20.5	
34	BJR-10	Dolostone	-0.3	20	
35	BJR-7	Calcite Marble	-3	23.6	
36	BJR-11	Calcite Marble	-3.3	16.1	
37	BJR-12	Calcite Marble	-3.7	5.3	

* data from Golani et al (2002)

carbonates are similar to those reported by Golani et al. (2002) from stratigraphically equivalent carbonates of Bhukia region that occur about 20 km south of Dugocha. The latter authors, depending on inferred homogeneity of four widely spread plots in $\delta^{13}C_{PDB}$ vs $\delta^{18}O_{SMOW}$ diagram (Fig.4), attribute the lighter carbon isotopic values to be of mantle origin and also compare the $\delta^{18}O_{SMOW}$ values of Bhukia carbonates with those from the carbonates of evaporate environment.

Although depleted $\delta^{13}C_{PDB}$ values in the range of -5 per mil are commonly attributed to the deeper mantle like sources, such values are also reported from many hydrothermal systems. The Dugocha data follows a diagenetic trend (Fig. 4) that is interpreted to represent either higher burial temperatures or under the influence of meteoric water (Burdett et al. 1990). Almost similar $\delta^{13}C_{PDB}$ isotopic values have been reported from carbonates of IOCG-type deposits like Olympic Dam (average $\delta^{13}C$ values of -2.6 ‰, Oreskes and Einaudi, 1990) and Wernecke (-4 to + 2 ‰, cf. Hitzman et al. 1992). This broad spectrum of carbon isotopic values is presumed to represent a mixture of carbon from carbonates of wall rocks, as well as hydrothermal or hydrothermally exchanged carbon. In such kind of deposits, it is further argued (Hitzman et al. 1992) that the REE concentrations have been introduced by hydrothermal fluids, and therefore may not necessarily be from deeper mantle sources (like alkaline rocks or carbonatites) at the sites of mineral deposition. Two most diagnostic features of the Dugocha carbonates are; (i) these are totally recrystallized with the constituent carbonate minerals

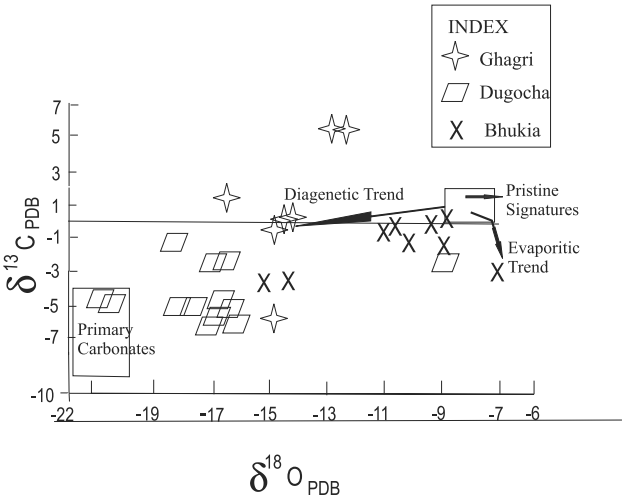

Fig.4. Carbon and oxygen isotopic plots for the Dugocha and Ghagri carbonates. Plots for Bhukia carbonates are from Golani et al. (2002). Field of pristine carbonate and trends of diagentic and evaporitic carbonates are from Burdett et al. (1990).

(calcite), silicates (albite, tremolite, chlorite and biotite) and decussately disseminated graphite flakes exhibiting distinct recrystallized and re-equilibrated granoblastic texture and (ii) the graphite flakes associated with feldspathic units have $\delta^{13}C_{PDB}$ values of around - 18 ‰ (Table 4). The latter values suggest that the precursor carbon of the graphitic flakes is of organic nature. Such organic carbon pervasively distributed in the carbonates must have significantly influenced the carbon isotopic values during metamorphic recrystallization. Therefore, we interpret the lighter $\delta^{13}C_{PDB}$ isotopic values of Dugocha carbonate as the result of pervasive intermixing of isotopically distinct carbon emanating from primary depositional carbonates, hydrothermally exchanged carbonates and also influence of organic carbon and their subsequent recrystallization under the conditions of burial temperatures. In Fig.4 it is significant to note that none of the samples plot closer to the trend defined by the carbonate rocks deposited in evaporitic environment.

MINERALIZATION

Cu-Au Mineralization

Grover and Verma (1993) reported for the first time visible gold in Bhukia area and high values of gold (up to 70 ppm Au) and copper (up to 2 wt.%) in few of the limonitised grab samples from the ancient working. This paved the way for the further exploration activity in Bhukia and its contiguous parts, particularly in structurally favored locations. Geological mapping, geochemical rock chip/ gossan sampling, stream sediment and soil geochemistry surveys, and preliminary diamond drilling helped in identification of several small size (= 1 Mt) lenses of gold ±copper±iron mineralization at (Anjeni, Ghagri, Dugocha, Isarwas, Bedawal, Manpura, Kukra areas) and a major gold-copper deposit near Bhukia. Most of these deposits open up at depth (Ghariya et al. 2001; Guha, 2004; Bejarniya and Kirmani, 2006) and significant mineralization along their strike extensions are still being reported. Bhukia is by far the largest deposit in this belt. Recently a larger tonnage of 60.58 Mt of gold @ 1.89 g/t Au inferred resource is reported by the Geological Survey of India (GSI, 2009).

Mineralization Styles and Ore Petrology

Ghagri Area: Geological map of the Ghagri prospect with plan locations and the cross sections of the representative bore holes (Fig. 5) show that the ore zones are localized in (i) feldspathic rocks (microclinites and albitites) and (ii) along the contact regions of massive dolomites with sheared and schistose dolomites. The ore

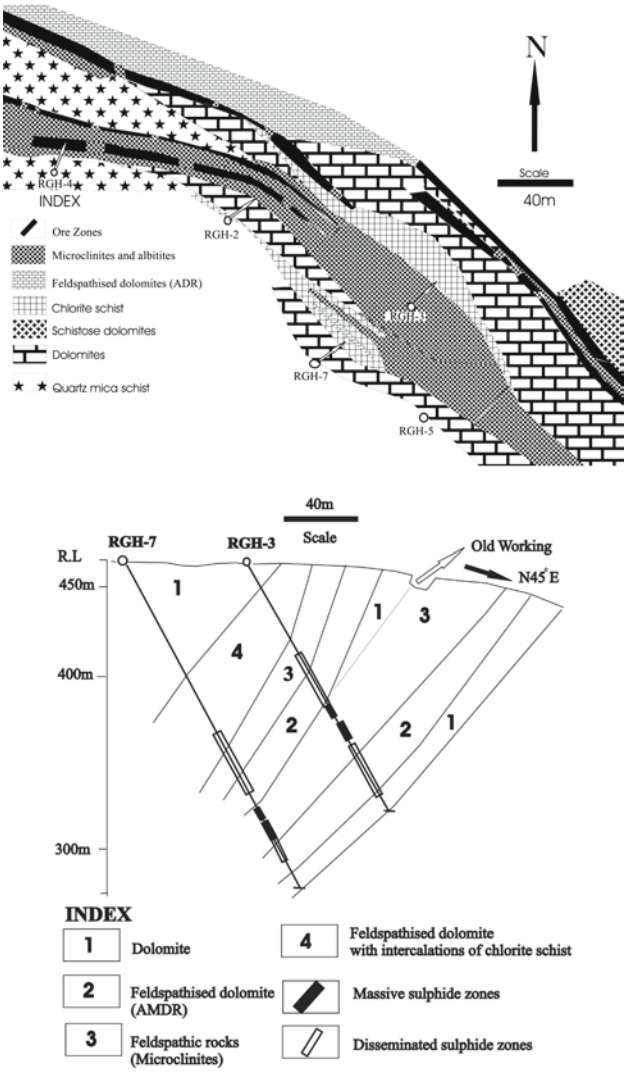

Fig.5. Geological map and representative bore-hole locations and sections of Ghagri Cu-Au-Fe prospect.

bodies are often seen transgressing the lithologic boundaries. The mineralization occur either in the form of semi-massive lenses, veins or as stringers. There is an increase in the thickness of the ore zones with depth. The ore zone is intensely brecciated (Fig.6A) with angular fragments of feldspathised dolomites, mineralized dolomites, and ore veins are tectonically intermixed and produce breccias on hand-specimen to outcrop scales. The carbonates away from the mineralized zones are comminuted to finer grained aggregates due to the effects of post-crystallization shear deformation. Carbonate minerals are ferroan dolomite to ankeritic dolomite in composition (with fairly good abundance of manganese, Table 2). These rocks are highly charged with opaque dust (made mainly of fine size hematite) and also with clusters of yellowish green biotites. Many of

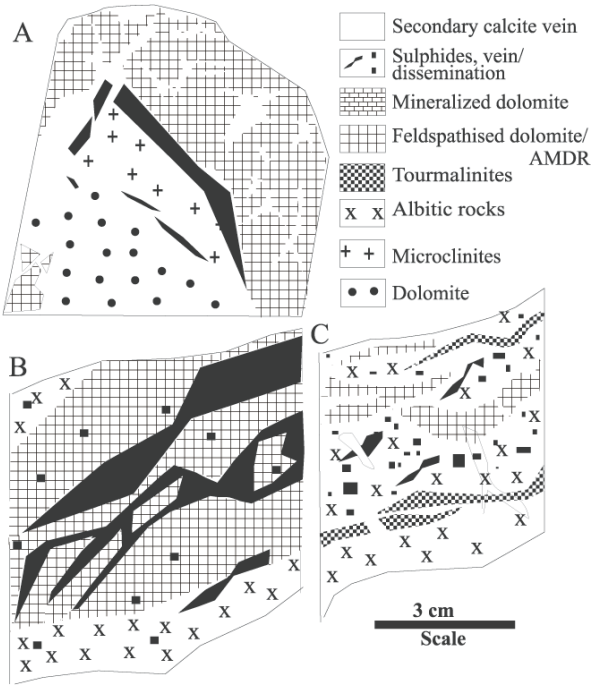

Fig. 6. Sketches drawn from drill-core cuttings from **A**. Ghagri, **B**. Dugocha, and **C**. Bhukia areas. For detail descriptions please see the text.

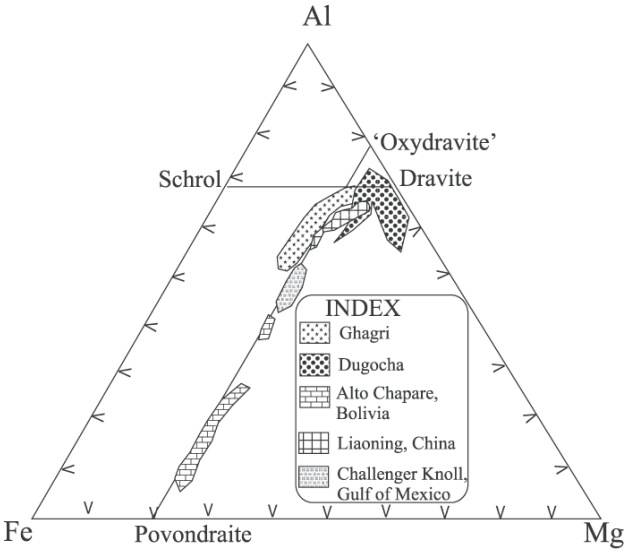

Fig.7. Al-Fe-Mg ternary diagram of tourmaline coposition. The Ghagri tourmalines plot along oxydravite-povondraite join, similar to the tourmalines from evaporite basins of Bolivia and China. The plots for tourmalines from Bolivia and China are from Henry et al. (2008).

the larger carbonates carry inclusions of tabular plagioclase crystallites. Tourmaline has a modal abundance that ranges between 10 volume % (in poorly mineralized rocks) and 40% volume (in highly mineralized rocks). The average chemical compositions of tourmalines from carbonates and from the mineralized carbonates are given in the Table 5 A and plotted in Al-Fe-Mg diagram (Fig. 7). An important observation from the data is that the tourmalines are less aluminous in nature and belong to povondraite-oxydravite series (Fareeduddin et al. 2010a).

Two phases of sulfide mineralization can be identified, an earlier phase, dominant in the form of, massive to semi massive ores mainly containing pyrrhotite with minor amounts of chalcopyrite and arsenopyrite (Fig.8A). Accessory amounts of pyrite associated with this sulphide phase occur as idiomorphic disseminations replacing magnetite grains, suggesting that some of the idiomorphic pyrite crystals represent the process of pyritization of magnetite. A later phase, often intensely brecciated, occurs in the form of cross cutting veinlets within the sulfides and also in the host rocks includes arsenopyrite, and minor chalcopyrite and pyrrhotite. Chalcopyrite is the main copper-bearing sulfide in both phases (Fig. 8D), though locally the presence of late bornite, ascribed to later phase of mineralization is recorded in a few bore holes. The idiomorphic arsenopyrite crystals contain exsolved phases of pyrrhotite (Fig.8B,C). Tiny blebs of ultra-fine gold particles (~ 10μ) occur in late phase fractured chalcopyrite. Magnetite, an important oxide phase in this rock, occurs as subhedral to subrounded disseminations. Many of the grains show embayed or corroded margins. Volume percent of magnetite in the rock range from 15% to almost about 30% in a few sections. Martitization of magnetite (patches and islands of hematite in magnetite) is very common.

Dugocha Area: Geological map of the Dugocha prospect with locations and the cross sections of representative bore holes (Fig. 9) indicate that the gold-sulfide ore is localized within tourmaline- graphite bearing albitites, along albite-microcline-dolomite rock (AMDR)/ calc silicates contact zones or within AMDR. The contact zones are intensely sheared and are characterized by mylonitic shear planes, silicification, brecciation and ferruginization. Sulfides, in the form of disseminations, thin discontinuous lenses and veins occur in 5 m and 30 m thick sulfide zones whose average sulfide concentration ranges between 5% and 60 % by volume (Fig.6B).

Sulfide minerals have well-defined granoblastic texture and polygonal outlines indicating annealing texture and recrystallization (Figs. 8E and 8F). The main sulfide minerals namely pyrrhotite and arsenopyrite with minor amounts of chalcopyrite occur in two parageneses. The earlier generation pyrrhotite is characterized by irregular grain boundaries and contains small amounts of pyrite derived as

Table 5A. Representative mineral chemistry of minerals from magnetite microclinites of Ghagri area

	K-feldspar					Albite						Magnesio-reibeckite			
	1	2	3	4	5	6	7	8	9	10	11	12	13	14	15
SiO_2	64.21	63.8	64.29	64.73	64.21	67.75	68.75	68.68	68.54	68.61	68.65	56.01	55.85	56.39	55.95
TiO_2	0.01	0	0	0.03	0	0	0	0.03	0	0	0	0.04	0.02	0.05	0.07
Al_2O_3	17.97	17.82	18.24	18.47	17.58	19.48	19.71	19.04	19.46	19.59	18.98	0.68	0.75	1.01	0.85
Fe_2O_3	0.06	0.09	0.04	0.14	0	0.81	0.04	0.08	0.04	0.11	0	16.99	16.78	12.1	14.12
FeO	NA	NA	NA	NA	NA	NA	NA	NA	NA	NA	NA	NA	NA	NA	NA
MnO	0	0	0	0	0	0	0	0	0	0	0	0.15	0.04	0.17	0.17
MgO	0	0	0	0	0.01	0	0.01	0	0.04	0.03	0.02	14.61	14.56	16.99	16.52
BaO	0.26	0	0	0	0.03	0	0	0	0	0.03	0	0		0	0
CaO	0	0	0	0	0	0.01	0	0.02	0	0.01	0	0.27	0.51	3.4	2.35
Na_2O	0.27	0.25	0.24	0.35	0.35	11.68	11.89	11.9	11.96	11.81	11.9	7.18	7.03	5.98	6.17
K_2O	16.8	17.19	16.83	16.76	16.78	0.06	0.06	0.1	0.08	0.13	0.09	0.23	0.16	0.3	0.25
Total	**99.58**	**99.15**	**99.69**	**100.5**	**98.96**	**99.79**	**100.5**	**99.85**	**100.1**	**100.3**	**99.64**	**96.16**	**95.7**	**96.39**	**96.45**
Si	2.998	2.996	2.99	2.99	3.01	2.974	2.99	3.006	2.99	2.99	3.01	7.96	7.964	7.92	7.89
Al	0.989	0.985	1.003	1.01	0.97	1.008	1.01	0.982	1.01	1.01	0.98	0.11	0.12	0.09	0.15
Fe^3	0.002	0.003	0	0	0	0.027	0.001	0.003	0	0	0	1.82	1.8	1.28	1.5
Ti	0.001	0	0	0	0	0	0	0.001	0	0	0	0.005	0.002	0.01	0.01
MgO	0	0	0	0		0	0	0	0	0	0	3.09	3.09	3.56	3.48
Na	0.024	0.023	0.02	0.03	0.03	0.994	1.003	1.01	1.01	0.998	1.01	1.96	1.92	1.49	1.64
Ca	0	0	0	0	0	0	0	0.001	0	0	0	0.04	0.08	0.51	0.36
K	1	1.029	0.999	0.986	1	0.004	0.004	0.006	0	0.01	0.001	0.041	0.029	0.54	0.45
Ba	0.005	0	0	0	0	0	0	0	0	0	0	0	0	0	0
Total	**5.019**	**5.036**	**5.02**	**5.01**	**5.02**	**5.008**	**5.008**	**5.009**	**5.02**	**5.01**	**5.01**	**15.03**	**15.01**	**15.4**	**15.48**
CN	0.005	0	0	0	0	0	0	0	0	0	0				
OR	0.972	0.978	0.979	0.969	0.969	0.004	0.004	0.006	0	0.01	0.01				
AB	0.024	0.022	0.02	0.03	0.03	0.996	0.996	0.994	0.996	0.992	0.995				
A N	0	0	0	0	0	0	0	0.001	0	0	0				

	Phlogopite		Spadaite	Magnetite		Rutile		Tourmaline		
	16	17	18	19	20	21	22	23*	24**	25***
SiO_2	41.73	41.7	30.6	0.06	0	0.13	0.13	35.00	36.06	35.01
TiO_2	1.21	1.08	0	0.239	0.275	98.14	96.55	0.34	0.65	0.58
Al_2O_3	12.72	12.25	16.66	0.009	0	0.04	0.04	24.99	28.64	25.89
Fe_2O_3	2.99	3.01	14.35	77.15	76.44	0.54	1.37	0.00	0.00	0.00
FeO				23.5	23.38			14.37	7.13	12.39
MnO	0.25	0.2	0.07	0	0	0.01	0.03	0.04	0.02	0.09
MgO	23.88	24.73	25.3	0.056	0.017	0	0	7.03	8.81	6.75
BaO	0.06	0	0	0	0	0.85	0.98			
CaO	0	0	0.02	0	0	0	0	0.74	0.32	0.47
Na_2O	0.12	0.09	0.02	0	0	0.04	0.02	2.46	2.70	2.57
K_2O	10.34	9.67	0.01	0	0	0.24	0.33	0.05	0.02	0.06
Total	**93.3**	**92.73**	**87.03**	**101**	**100.1**	**99.99**	**99.45**	**85.00**	**84.36**	**83.81**

* = Average of 8 sulphide hosted tourmalines; ** average of 15 dolomite hosted tourmalines; *** average of 5 albite-carbonate tourmalines

its alteration product. The late pyrrhotite occurs as idiomorphic grains along small size veinlets. Such pyrrhotites possess exsolved phases of cubanite (Fig. 8G). The microbeam analyses of the pyrrhotite (Table 6) indicate that despite uniform compositional range, chemical distinction between early and late phase pyrrhotite is possible in terms of presence of nickel (0.29 to 0.39 wt %) and about 1-2% less Fe in the former phase of pyrrhotites. Small quantities of anhedral chalcopyrite are present. Pyrite, an early sulphide phase is also significantly enriched in nickel (0.89 wt%). Some of these pyrites show slight anisotropism indicating transition to late phase arsenian pyrite or arsenopyrite. The early phase arsenopyrite occurs in the form of anhedral, angular and brecciated grains whereas the dominant late phase arsenopyrites occur as idiomorphic grains in veinlets. Arsenic content in early phase arsenopyrite (Table 6) ranges from 45.49 to 46.62 wt. % whereas it varies between 47.56 wt % and 52.84 wt % in the later phase. An important feature of the late phase arsenopyrite is significant enrichment of Co and Ni (Table 6: 0.06 to 2.34 wt % Co

Table 5B. Co-existing albite-microcline-dolomite in AMR, Ghaghri area

Analyses No.	1 Alb-R 8/72akf	2 Ortho-C 7/72akf	3 Dolo 37/72akf	4 K-feld-R 38/72akf	5 K-feld-C 39/72akf	6 Alb-C 40/72akf	7 K-felds-I 41/72akf	8 Alb-R 42/72akf	9 Dolo 43/72akf	10 K-feld-C 44/72akf	11 K-feld-R 45/72akf
SiO_2	67.49	63.58	0.02	63.4	63.18	67.81	63.52	67.54	0	63.8	63.62
TiO_2	0	0.01	0	0.04	0	0	0	0	0	0.01	0.03
Al_2O_3	18.92	17.88	0	18.21	18.04	19.39	18	19.18	0.03	18.37	18.32
FeO	0.06	0.06	1.02	0.14	0.07	0.17	0.12	0.07	1.06	0.27	0.3
MgO	0	0	21.2	0.02	0.02	0	0	0	22.37	0	0.02
CaO	0.07	0.03	29.27	0.01	0.02	0.07	0.02	0.03	31.6	0.01	0
Na_2O	11.3	0.16	0.01	0.31	0.35	11.35	0.43	11.24	0.02	0.21	0.11
K_2O	0.13	16.49	0.04	16.03	16.28	0.18	16.27	0.13	0	16.18	16.29
P_2O_5	0	0	0.29	0	0	0	0	0	0.27	0	0.04
Cr_2O_3	0	0	0.03	0.05	0	0	0.01	0	0	0.01	0
MnO	0.1	0.06	0.59	0.01	0	0	0	0	0.62	0.02	0.02
NiO	0	0	0.03	0	0.02	0	0	0.01	0.03	0	0
BaO	0.07	0.23	0	0.1	0	0	0	0	0	0	0
Total	**98.14**	**98.49**	**52.5**	**98.31**	**97.97**	**98.96**	**98.36**	**98.2**	**56**	**98.88**	**98.76**

Analyses numbers are shown in the back scattered image.
Analysis 8 is rim to the core of K-felds shown in analyses 7
Analysis 37 is carbonate bordering K-feld
Analysis 38 K-felds rim bordering carbonate
Analysis 39 K-feld core
Analysis 40 is Albite bordering K-feld
Analysis 41 is K-felds inclusion in albite
Analysis 42 is host albite rim
Analysis 43 is carbonate bordering albite
Analysis 44 is K-felds Core
Analysis 45 is K-feld Rim

Abbreviations used: Alb-R =Albite Rim; Alb-C = Albite Core; K-fled-R = K-feldspar Rim; K-feld-C = K-feldspar Core; Dolo = Dolomite. K-feld-I = K-feldspar Inclusion

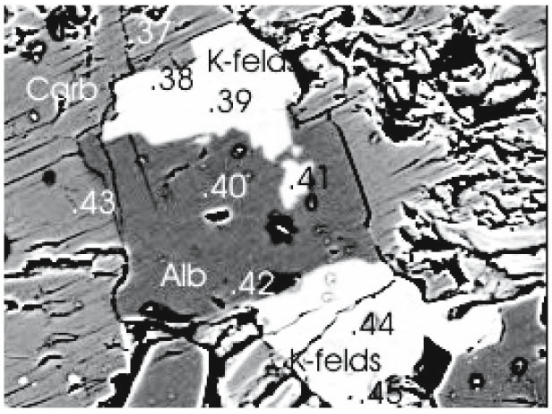

and 0.09 to 1.55 wt % Ni, one sample show very high Co and Ni i.e 22.09 and 3.37 wt % respectively). A few of the arsenopyrites are cupriferous (up to 8.44 wt % Cu, Table 6). Chalcopyrite analyzed up to 34.62 wt % copper. Late phase pentlandite is recorded along the granoblastic grain boundaries of pyrrhotite (Fig. 8 F). Nickel contents in pentlandite is highly variable and ranges from 10.08 to about 32.64 wt.%. The low nickeliferous varieties are richer in iron than sulfur. Bismuth-bearing minerals often constitute important mineral phases in the sulfide zones (Fig. 8E). These occur either as yellowish white occluded grains in arsenopyrite with polishing scratches or as droplets or even as resorbed stretched grains at the grain boundaries of other sulfide grains. The bismuth phases (Table 6) include bismuth-telluride (wherlite), bismuth-copper sulfo-salts (wittichenite?) and almost pure native bismuth. Association of graphite flakes with sulfides is very common. Gold occurs in native form as tiny grains (about 10 microns) within arsenopyrite. Native form of electrum and auricupride in association with Bi-bearing mineral phases that consist of bismuth-telluride and almost pure native bismuth is also recorded (Table 6).

Bhukia Area: The mineralized zones at Bhukia (Fig. 10) are intimately intermixed with angular to subangular fragments of sulfide-bearing carbonates, albitites, and tourmaline rich pockets (tourmalinites, Fig.6C). Beside dolomite, the carbonate fragments in the ore zones contain actinolite, scapolite, biotite, titanite and fine graphitic grains The structure of the deposit is defined by pervasive $S_0 = S_1$ schistosity that are refolded along a major steeply plunging (70° to 76° towards NNW or SSE) second generation synformal structure. Whereas the western limb of this fold is normal with its sympathetic folds, the eastern limb is attenuated and dragged along the NNW-SSE trending shear zone. The auriferous disseminated to semi-massive sulfides exhibit discordant relationship with schistosity ($S_0 = S_1$) and occur in two distinct structurally favorable loci. These are (i) along the axial zones of the second generation structure as plunging ore shoots; the ancient miners apparently

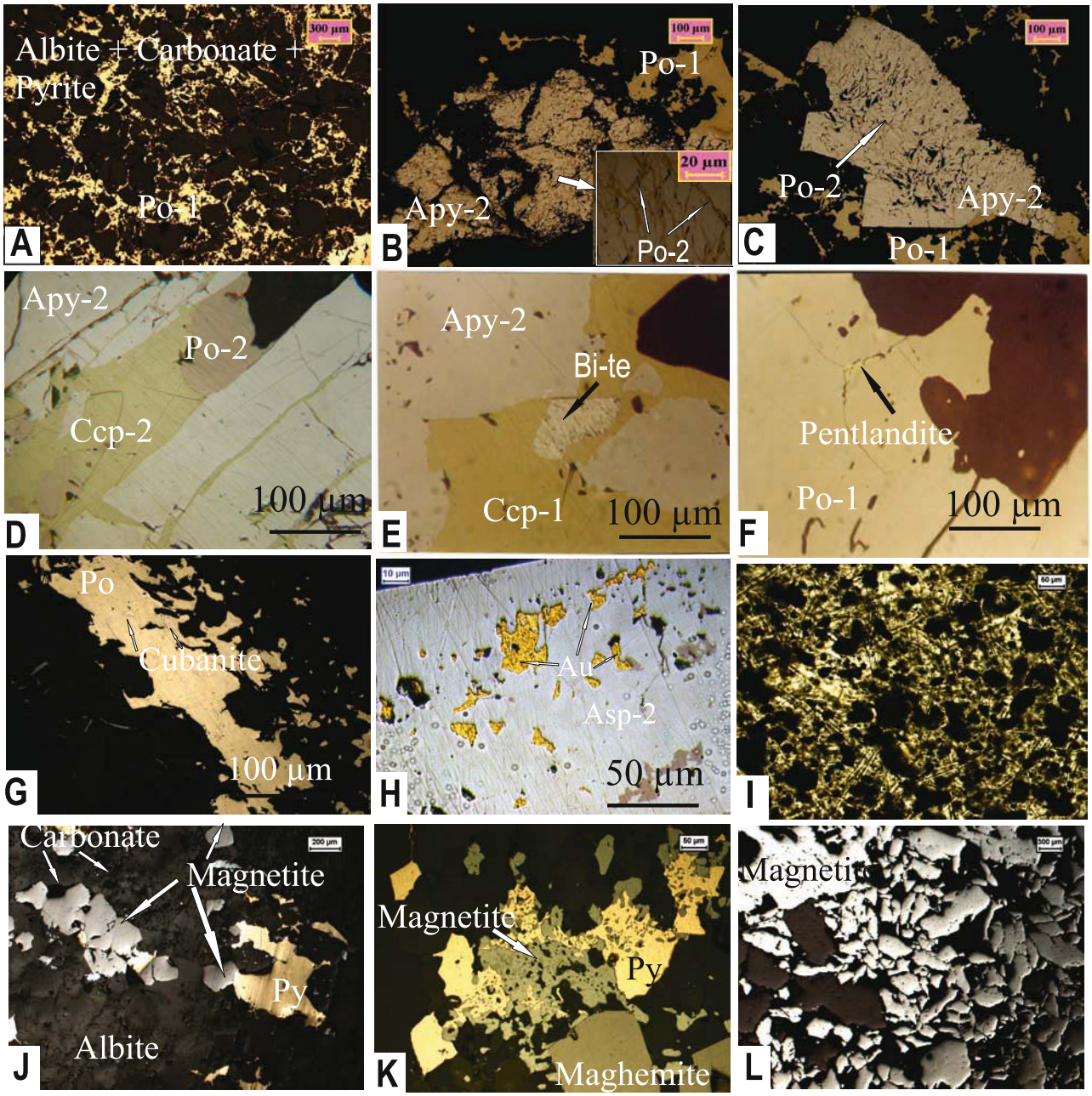

Fig. 8. Photomicrographs of the ore-sections from Salumber-Ghatol sector. **A**. An intensely brecciated semi-massive pyrite ores occurring at the interstices of angular fragments of AMDR. **B**. Cataclastically disintegrated early phase arsenopyrite; note development of intense pyrrhotite veinlets (inset) within arsenopyrite **C**. A large porphyroblast of early phase arsenopyrite (Asp). Note granoblastic grain margin (NW and SW corner) and lobate grain margin (NE corner) of the same porhyroblast. **D**. Second generation veins of pyrrhotite and chalcopyrite traversing arsenopyrite. **E**. Idiomorphic grains of bismuth-telluride (Bi-Te) and arsenopyrite in chalcopyrite. **F**. Pentlandite grains developed along the triple point junctions of a large pyrrhotite grain. **G**. Exsolved phases of cubanite in pyrrhotite; H. Trails of anhedral gold grains in arsenopyrite. **I**. Dissemination of magnetite in magnetite-microclinite of Ghagri area. Transmitted plane polarized light. **J.** Magnetite disseminations in AMDR rocks. Note the recrystallized grain boundaries of magnetites. **K**. Pyrite replacing earlier generation magnetite. Note the development of late ideoblasts of maghemite and presence of anhedral patches of hematite within magnetites. **L**. Hematite breccia from Manpur area.

Table 6. Electron microprobe analyses of sulphide phases from Dugocha deposit

	Pyrrhotite (Early Phase)				Pyrite		Pyrrhotite Late Phase										Pentralndite				
	1	2	3	4	1	1	2	3	4	5	6	7	8	1	2	3	4	5	6	7	8	9
S	38.52	39.09	38.07	38.23	53.05	34.9	38.47	38.35	38.39	38.5	38.22	38.03	38.83	33.31	37.42	34.26	34.64	33.88	33.97	35.52	32.5	35.18
Fe	59.04	59.36	59.36	58.4	44.94	59.7	60.69	60.34	60.96	60.02	60.27	60.17	60.17	33.17	50.86	39.49	41.26	37.4	36.95	41.83	32.22	42.59
Co	0.03	0.02	0.04	0.05	0.08	0.02	0.01	0.06	0	0.05	0.09	0.04	0.04	1.13	0.47	1.05	0.93	0.89	1.12	0.96	1.4	0.54
Ni	0.39	0.29	0.3	0.38	0.89	0.39	0.05	0.08	0	0	0	0.02	0.02	31.63	10.08	21.96	21.26	26.45	27.44	21.29	32.67	20.2
Cu	0	0	0	0.38	0.07	0.01	0.04	0	0	0.04	0	0	0	0.01	0	0.01	0	0	0	0	0	0
Zn	0	0	0	0	0	0.07	0	0	0	0	0	0	0	0	0	0	0	0	0	0	0	0
As	0	0	0	0	0.06	0	0	0	0	0	0	0	0	0	0	0	0	0.05	0.03	0.05	0	0.06
Se	0	0	0	0	0	0.04		0	0	0.05	0	0	0	0	0	0	0	0	0.15	0	0	0
Ag	0.07	0	0	0	0	0	0.04	0	0	0.06	0	0	0	0	0	0	0	0	0	0.07	0	0
Sb	0	0	0.02	0	0	0	0.24	0	0	0	0	0.03	0.03	0	0	0.04	0.05	0.01	0	0	0	0
Te	0	0	0	0.04	0	0	0	0	0	0	0.01	0	0	0	0	0.06	0.02	0.01	0	0.11	0.04	0.01
Au	0.09	0	0.07	0	0	0	0.03	0.18	0.12	0	0	0	0	0	0	0	0	0	0	0	0	0
Bi	0	0	0	0	0	0	0	0	0	0	0.23	0	0	0	0	0.11	0	0	0	0.09	0	0
Pb	0.19	0.07	0.25	0.33	0.13	0.17	0.06	0.03	0.28	0.13	0.18	0	0.03	0.19	0	0.09	0.04	0.17	0	0.08	0.1	0
Total	**98.33**	**98.83**	**98.11**	**97.81**	**99.22**	**95.3**	**99.63**	**99.04**	**99.75**	**98.85**	**99**	**98.29**	**99.12**	**99.44**	**98.83**	**97.07**	**98.2**	**98.86**	**99.66**	**100**	**98.93**	**98.58**

																			Bismuth bearing phases						
	Chalcopyrite				Arsenopyrite Earyl Phase						Arsenopyrite Late Phase								Co-ASP	Cu-ASP	Bismuthunite		Wittichenite?		Wherlite	
	1	2	3	4	1	2	3	4	5	6	7	10	11	12	13	14	15	8	1	2	3	1	2	1	2
S	34.17	35.37	34.33	35.3	19.78	20.87	19.55	19.83	15.93	17.16	17.46	16.99	18.51	16.62	19.79	18.48	10.27	20.21	2.27	7.23	30.03	27.26	16.99	0.38	1.93
Fe	30.13	29.89	30.25	28.89	34.13	34.66	34.06	33.55	29.9	31.94	32.44	31.66	32.43	30.66	32.62	31.2	8.08	32.15	0.31	0	0.43	6.92	31.86	3.72	10.75
Co	0	0	0.03	0	0.5	0.09	0.06	0.06	2.34	2.11	1.75	2.06	1.23	1.98	0.98	1.45	22.09	0.6	0.05	0.04	0.01	0	0	0.46	1.27
Ni	0	0	0.03	0	0	0.09	0	0	1.55	0.09	0.17	0.18	0.31	1.05	0.1	0.45	3.37	0.13	0	0	0	0	0	0.1	0.26
Cu	34.62	34.21	34.36	34.21	0	0.04	0	0.55	0	0.02	0.02	0.03	0.28	0.03	0	0.86	0	8.44	1.48	4.18	0.31	18.91	19.21	8.91	0
Zn	0.04	0	0	0	0	0	0.04	0	0	0	0	0	0	0	0	0	0	0.07	0	0	0	0	0	0	0.1
As	0	0.01	0.02	0.01	46.03	46.61	46.62	45.49	50.13	49.7	49.34	50.09	46.99	51.18	47.56	47.63	52.84	39.93	0	0	0	0	0	3.28	7.01
Se	0	0	0	0	0	0	0	0	0	0	0	0	0	0	0.12	0	0	0	0	0	0	0	0	0	0
Ag	0	0.11	0.05	0.11	0	0	0	0.05	0	0	0	0	0	0	0	0	0.05	0	0	0	0	0	0	0	0
Sb	0	0	0	0.04	0	0.04	0.02	0	0	0	0	0	0	0	0.04	0.01	0.11	0.02	0.62	0.26	0.25	0.08	0.09	0.08	0.1
Te	0	0	ND	ND	0	0.09	0	0	0.03	0	0	ND	ND	0	0.09	0	0	0	-	-	0	0	-	28.23	35.72
Au	0	0.01	0	0	0	0.1	0	0	0.03	0	0	0	0	0.2	0.1	0	0	0	0.13	0	0.09	0.24	0.16	0.24	0.11
Bi	0	0	0	0	0	0	0	0	0	0	0	0	0	0	0	0	0	0	93.24	86.78	65.38	48.57	31.85	53.34	41.21
Pb	0	0	0	0.14	0.03	0.06	0	0	0.14	0	0.03	0.21	0.12	0.19	0.14	0	0.12	0	1.9	0.92	1.32	0.95	0.63	1.91	1.49
Total	**98.96**	**99.6**	**99.07**	**98.7**	**100.47**	**102.65**	**100.35**	**99.53**	**100.05**	**101.02**	**101.21**	**101.22**	**99.87**	**101.91**	**101.54**	**100.08**	**96.93**	**101.55**	**100**	**99.41**	**97.82**	**102.93**	**100.79**	**100.65**	**99.95**

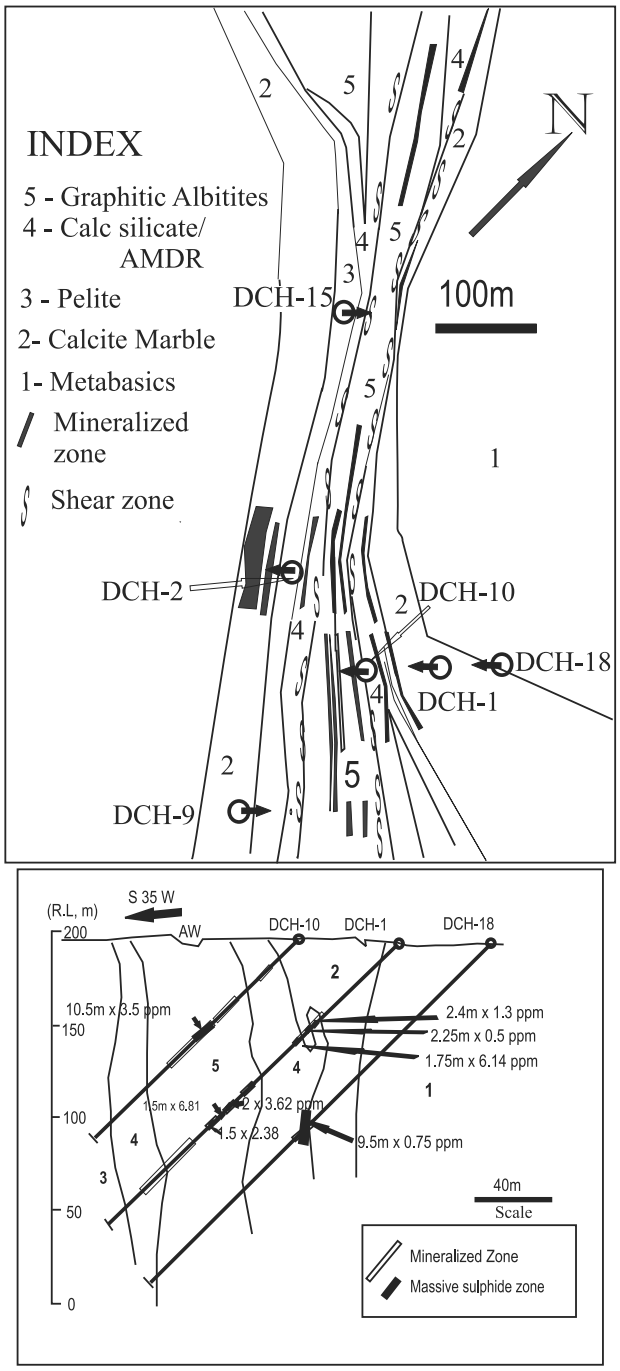

Fig.9. Geological map and representative borehole locations and cross sections of Dugocha Cu-Au prospect.

exploited the auriferous lodes that are oriented along the plunge as pitch of the ancient workings and the plunge of F2-folds show striking coincidence (ii) innumerable discontinuous lenses of varying dimensions towards eastern sector along the NNW-SSE trending shear zones that developed during the waning phase of the second generation deformational structures. The latter ore bodies are flattened and often telescoped one into another. Ore-microscopic studies confirm the field evidence of preferential localization of sulfide along S_2 cleavage planes. Small size stringers/ veinlets, veins and dissemination of sulfides occupying intergranular spaces and along 2nd generation shears and axial planar fractures gave rise to stock work pattern, which gradually converged to form massive sulfide zones (Ghariya et al. 2001). Guha (2004) has reported mylonite zones with S-C fabric, stretching lineations, stretched augens with delta-shaped trail and sheath structures in the eastern block of the Bhukia gold-copper deposit.

The mineralization comprises of pyrrhotite, chalcopyrite, arsenopyrite, magnetite, loellingite, cubanite, bornite, covellite, pyrite, Bi-bearing phases (maldonite, wherlite), cobaltite, bornite, gold tellurides, native bismuth, and gold/ electrum. Among the two phases of mineralization the first phase is represented by coarse-grained massive and cataclastic sulfide assemblage generally forming ore breccias with (i) angular fragments of quartz, albitic feldspar, carbonate, and tourmaline rich feldspathic units, (ii) extensively fractured and brecciated megacryts, (iii) deformed twin lamellae and (iv) deformed and twisted silicate phases either along the interstices or within the sulfide grains. The second phase of mineralization occurs as close-spaced fracture filling veins. The latter is intimately associated with the secondary amphiboles, chlorite, tourmaline, and calcite. Arsenopyrite, pyrrhotite, and chalcopyrite are the mineral phases that dominate in both phases of sulfide mineralization, whereas minor phases like cubanite, bornite, covellite, bismuth, and gold tellurides and native bismuth could be related to the second phase of mineralization. Higher values of gold in the samples where second phase of mineralization is dominant, particularly in proximity of secondary carbonate veins, attest to the late deposition of gold during the mineralization history of the deposit (Guha, 2004). Native gold occurs in variable shape and size (usually between 10 to 1000 microns) in second phase arsenopyrite (Fig.8H), chalcopyrite, bismuth, and rarely pyrrhotite. The common gold shapes are various combinations of triangles, lozenge, rhombs, needle/ dendroids and droplets. Gold pseudomorphs after arsenopyrite are common. In alteration zones with sparse sulfides, the idiomorphic to circular droplets and fine dust-sized gold particles of native gold occur along micro-fractures. Very often larger flakes of visible gold could be seen in the hypogene alteration zone where the yellow metal in altered goethite or iron-rich jaspery material could easily be recognized. Micro-fractures containing composite veins of chalcopyrite, gold, and gangue material invariably occur in cataclastic arsenopyrite. Bismuth and several gold-

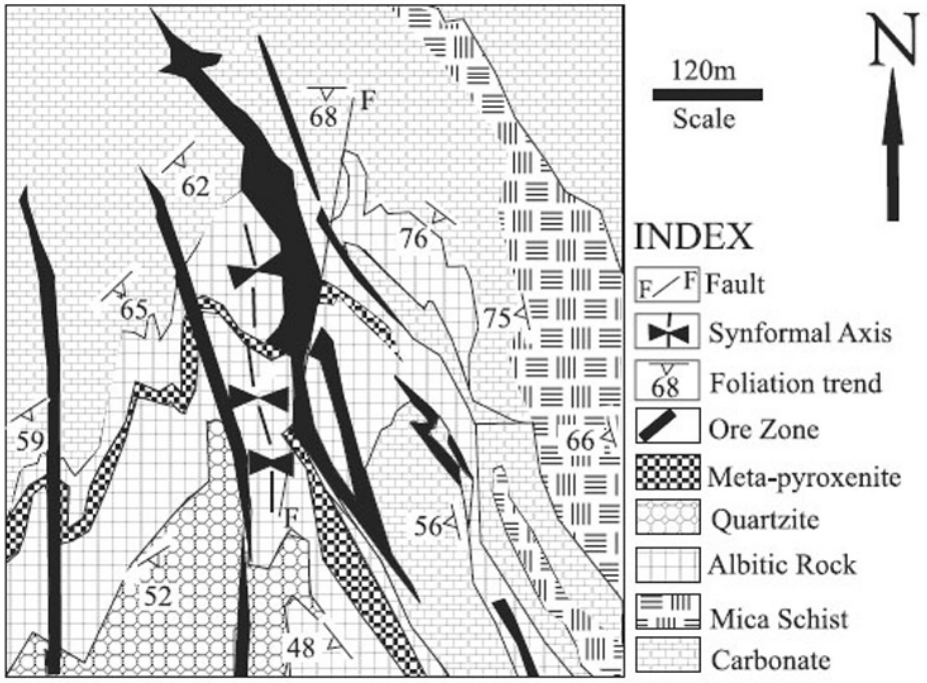

Fig. 10. Geological map of Bhukia Cu-Au deposit (modified after Ghariya et al. 2001).

tellurides occur in close association with native gold. Electron microcprobe analyses of gold grains from the Bhukia area revealed that the gold content ranges between 92.23 % and 98.47 wt.%, while silver content varies from 3.65 wt.% and 6.55 wt.% (Golani et al. 1999). Gold is of very high fineness of about 950 (Ghariya et al. 2001; Guha, 2004).

ALTERATION ZONES

Ghagri area: The alteration zones are represented by the extensive development of rocks that contain feldspar, carbonate and magnetite as essential minerals whose relative volume percent depends on the proximity with the mineral lodes and help in classifying two variants namely (i) distal magnetite microclinite rock and (ii) proximal albite-microcline-dolomite rocks (AMDR).

The magnetite-microclinite rocks are grey and pink coloured (Fig.11A), cryptocrystalline with microcline, magnesio-reibeckite, magnetite/maghematite, and phlogopite as essential minerals. Small amounts of carbonate, tourmaline, biotite, titanite, apatite, quartz, and rare muscovite are present in different variants of the rock. Untwinned and unaltered finely crystalline (10 μ to 50 μ size), microcline albeit with diffused grain boundaries is the most dominant mineral whose modal abundance ranges from about 75 percent of the rock (Fig.11B) to becoming almost a mono-mineralic microclinite (> 90 % of microcline,). It analyzes to its purest form (K_2O content from 16.8 wt. % to 17.19 wt. %, Table 5) with Or-molecule in excess of 0.969. The microclinites contain minor to trace amounts of albite ($Ab_{0.992}$ to $Ab_{0.996}$). Randomly oriented acicular crystals of pale green to bluish green magnesio-riebeckite (Fig. 11 B, Table 5A) represent dominant mafic mineral in the rock. Carbonates in veins are coarsely crystalline and sometimes also occur as discrete disseminated grains. Flakes of yellowish brown to deep brown mica, purple and deep blue tourmaline occur in trace amounts. Mica is a low alumina phlogopite (Fig. 11B, Table 5A) and co-exists with flaky hydrous magnesium silicate compositionally closer to the mineral species spadaite (Table 5A). Quartz is either totally absent or occurs in accessory amount. Spinels in these rocks are mainly magnetite and maghemites (Fig. 8K, Table 5A).

Intimately associated with the microclinites and constituting the immediate host for bulk of the mineralization are the albite-microcline-dolomite-magnetite rocks that additionally contain variable contents of dolomite and albite, making these rocks either as albite-microcline rocks (AMR, Fig. 11 F) or albite-magnetite-dolomite rock (AMDR, Fig. 11 D). The AMR are coarse-grained equi-granular, hypidiomorphic, grey coloured rocks with minerals in decreasing order of abundance as albite, K-feldspar, carbonates, magnetite, tourmaline, biotite, titanite, and apatite. Both Na- and K- feldspars exhibit remarkable uniformity in their composition with no zoning. Biotite is phlogopitic and carbonate is dolomitic. There is an intimate

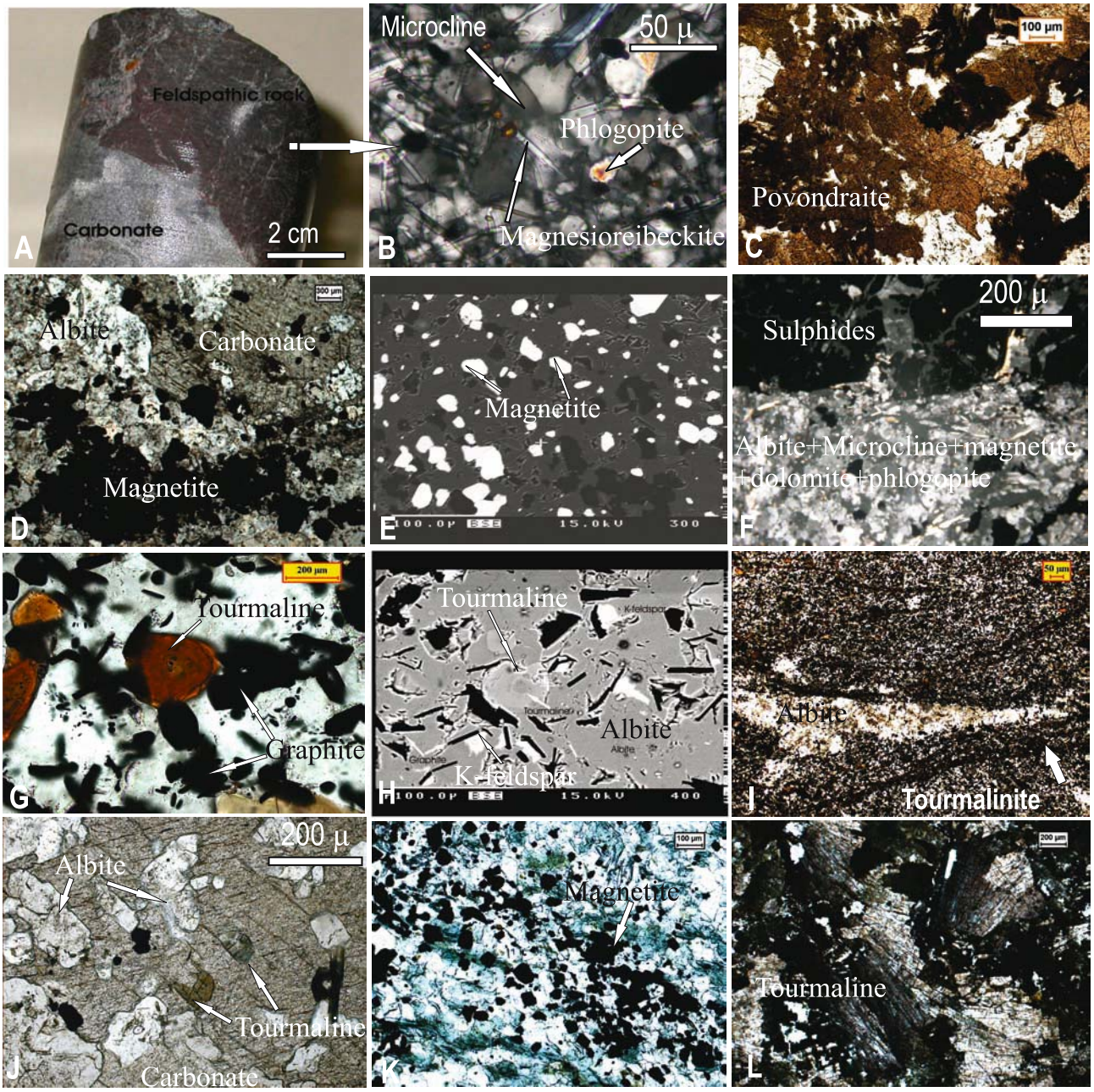

Fig. 11. Drill core photograph, photomicrographs and SEM-backscattered electron images showing different petrographic features from the alteration zones of Ghagri (A to F), Dugocha (G to I) and Bhukia (J to L) mineral deposits. **A**. Drill core photograph showing the contact relationship of dolomite and microclinite. Note the fine network of secondary carbonate (white) traversing the carbonate-microclinite contact zones and also within the microclinites. **B**. Microclinite showing granoblastic aggregates of very fine grained untwined microcline, randomly oriented acicular magnesioriebeckite and flaky phlogopite. **C**. Povonderitic tourmalines in mineralized zones. **D**. Anhedral and embayed crystals of albite, large size grains of carbonate and magnetite in AMDR. **E**. BSE image showing disseminations of magnetite (bright), albite (grey) and carbonate (dark grey) in albite-magnetite-dolomite rock (AMDR) **F**. Sulfide vein traversing AMR. . **G**. Tourmaline and graphite in albitites. **H**. BSE image showing tourmaline, albite, K-feldspar and graphite in albitites. **I**. Veinlets of tourmalinites (dark colored) alternates with veinlet of albitites (white) in tourmaline-graphite albitites. **J**. Inclusions of albite and tourmaline in large megacryst of carbonate. **K**. A magnetite layer traversing albite-amphibole rock. **L**. Cluster of povondraitic tourmaline in mineralized albitites rock. The photomicrographs B and F are under cross nicols, and the rest are under plane polarized transmitted light.

intergrowth of albite, K-feldspar and carbonates in these rocks manifested by (i) K-feldspar mantled by a rim of albite; (ii) larger grains of albite containing inclusions of K-feldspar, and (iii) large carbonate crystals enclosing albitic plagioclase and vice versa. Table 5B lists the analyses of the co-existing mineral phases from AMR separately and similarity of composition with ADMR and lack of zoning is apparent. Tourmaline (Fig. 11C) and magnetite (Fig. 11D) are important constituents of these mineralized carbonate-feldspar rocks. The rock also contains fine-grained granular quartz, albeit in accessory amounts. Green biotite occurs in clusters, defines a crude foliation and very commonly is either chloritised or occurs as bleached masses.

Dugocha-Bhukia area: The alteration zone in Dugocha deposits is represented by a very fine-grained dark grey, dull luster graphitic albitites that occurs as conformable band within dolomitic marble. Its thickness varies between 50 m to 100 m and has an exposed length of over 3 km. Petrographically two distinct variants of this rock could be recognized namely (i) graphitic albitites containing 20μ to 30μ size granoblastic mosaic of untwinned albite (modal abundance 50-80%, sometimes reaching up to 95%), amorphous looking carbonaceous matter (10% to 30%) and tourmaline (5-15%, Fig.11G); (ii) albite-microcline rocks (AMR) that possess, in addition to above minerals, substantial amount of K-feldspar (Fig. 11H). Locally carbonaceous matter may exceed 60 volume percent of the rock. Accessory minerals include sulfides, tremolite, granular magnetite, and rare allanite, with rutile and quartz. In AMR, the amount of K-feldspar sometimes is highly variable and locally may even exceed albite. The most characteristic feature of the rock is the intimate intergrowth of silicates and carbonaceous matter either in a decussate fashion (Fig.11 G, H) or rarely, as stretched grains defining fine foliation in the rock. The electron microprobe analysis of the feldspathic mineral (Table 7) suggests (i) virtual absence of intermediate members of Na-K solid solution series and (ii) lack of zoning in feldspars. The K-feldspars in AMR occur as individual grains with irregular grain boundaries (Fig. 11H). Deep reddish brown, fine- to medium-grained (20 to 40 microns) and well-rounded zoned dravitic tourmalines (ZT, Fig.11H) that are at some places concentrated in the form of fine-size tourmalinite laminae (Fig. 11I) bordering albitites lenses are most ubiquitous in the mineralized zones. Fareeduddin et al (2010b) have provided detailed description of the tourmalines in the Dugocha mineralized zones. Important conclusions from this study are (i) tourmaline cores are

Table 7. Representative electron microprobe analyses of minerals from albite-graphite-tourmaline rock of Dugocha area

	Albite			K-feldspar			Tourmaline				Sphene
Sl. No.	1	2	3	4	5	6	7	8	9	10	11
An. No.	7	8	9	48	37	42	45	54	55	56	22
SiO_2	68.67	67.33	66.91	65.82	64.83	64.06	64.546	36.83	37.99	37.33	29.96
TiO_2	0.01	0.01	0	0	0	0	0	2.52	0.3	2.06	39.86
Al_2O_3	19.3	20.23	19.83	21.2	18.12	18.32	18.5	27.79	31.3	28.69	1.06
Fe_2O_3	0	0.01	0.19	0	0.08	0.02	0.03	4.57	3.81	8.91	0.06
MnO	0	0	0	0	0	0	0	0	0	0.05	0
MgO	0	0	0	0	0	0	0	10.48	8.89	10.16	0
BaO	0	0.04	0	0	0	0	0.14	0	0	0	0.1
CaO	0.26	0.9	0.94	2.5	0	0	0	1.87	0.16	1.39	28.53
Na_2O	11.49	11.18	11.07	10.28	0.23	0.45	0.46	2	2.92	2.27	0.02
K_2O	0.03	0.1	0.11	0.15	16.64	16.31	16.12	0.03	0	0.05	0.03
Total	**99.76**	**99.8**	**99.05**	**99.95**	**99.9**	**99.16**	**99.8**	**86.09**	**85.37**	**90.91**	**99.62**
Si	3.003	2.954	2.959	2.895	3.004	2.991	2.991				
Al	0.995	1.046	1.034	1.099	0.99	1.008	1.011				
Fe3	0	0	0.006	0	0.003	0.001	0.001				
Ti	0	0	0	0	0	0	0				
Na	0.975	0.951	0.949	0.877	0.019	0.041	0.41				
Ca	0.012	0.042	0.045	0.118	0	0	0				
K	0.002	0.005	0.006	0.008	0.984	0.971	0.953				
Ba	0	0.001	0	0	0	0	0.003				
Total	**4.987**	**4.999**	**4.999**	**4.997**	**5.001**	**5.011**	**5**				
CN	0	0.001	0	0	0	0	0				
OR	0.002	0.005	0.006	0.008	0.981	0.96	0.003				
AB	0.986	0.952	0.95	0.874	0.019	0.04	0.956				
AN	0.012	0.042	0.045	0.118	0	0	0.041				

significantly richer in chromium and (ii) the tourmalines show affinity to the tourmalines of the Fe^{3+} quartz tourmaline rocks. The cryptocrystalline graphite has a modal abundance of 2-30 (1.5 wt % to almost about 9 wt. %). The isotopic analyses on two samples analyzed $\delta^{13}C_{PDB}$ -18 to - 20 per mil (Table 4) indicating the carbon to be organic in origin.

Bhukia area: Albite-rich rocks constitute bulk of the alteration zones in Bhukia area (Fig.10). Besides albite, these rocks also contain various proportions of actinolite, hornblende, tourmaline and carbonate minerals. Depending on their relative volume percent these albite- rich rocks can be classified as albitite (pure albite in excess of 80% volume percent), albite-amphibole-magnetite rocks (almost equal proportion of these minerals, Fig. 11K), albite carbonate rocks, albite-tourmaline rock and tourmalinites. These variants inextricably mixed with each other in different prospect/deposit. The dominant mineral albite is largely untwinned and very commonly exhibits diffused grain margins. Actinolite and hornblende show alteration to chlorite. Calcite and titanite occur as discrete grains. Tourmaline occurs in several paragenesis that include: (i) very fine size tourmalines that occur in thinly laminated tourmalinite layers (1-5 mm) that alternate with quartz + feldspar and chlorite + biotite layers. These exhibit color zoning in the form of dark brown cores and pale brown rims. (ii) Discrete euhedral grains of un-zoned green tourmalines are ubiquitous in mineralized feldsapthic rocks. (iii) Highly corroded grains of prismatic green tourmalines in plagioclase-carbonate rocks (Fig. 11J). (iv) In radiating clusters of coarse fractured tourmaline that are dichroic between pale yellowish purplish brown to deep brown shades (Fig. 11 L). The brown tourmalines from paragenesis tourmaline + quartz + plagioclase ± epidote + chlorite + biotite + calcite + titanite + sulphides exhibit higher concentration of MgO, and TiO_2, with X_{Mg} values (0.132 to 0.33) that are comparable to the higher X_{Mg} values of Dugocha tourmalines (Fareeduddin et al., 2010b) and with the chemistry of tourmalines from an evaporitic environment of the Liaoning area, China (Fig. 7; Henry et al. 2008).

Mineral paragenesis: A summary of the paragenetic sequences as deduced from the textural features of the constituent mineral phases in these three deposits is presented in Fig.12. The major mineral phases present in all the three deposits studied are broadly similar, albeit their relative abundances differ significantly. The sulfide assemblage is essentially free from Pb-Zn phases. Quartz occurs in minor amounts and does not constitute significant part of the alteration mineralogy. An early and a late stage

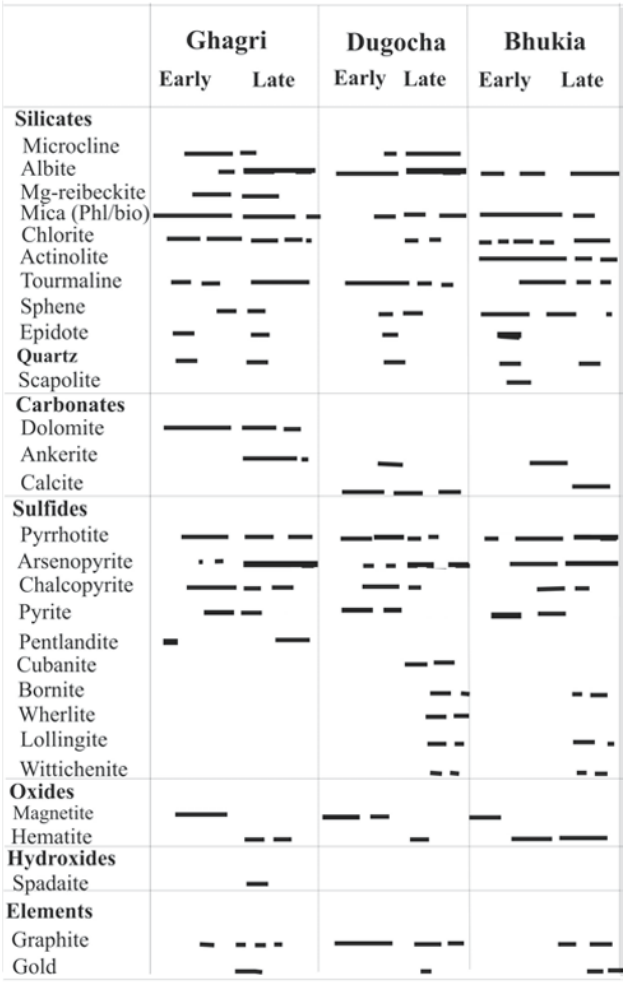

Also present late phase electrum (Dugocha) maldonite, covelite, chalcosite, brucite and uraninite (Bhukia)

Fig. 12. Mineral paragenesis in Ghagri, Dugocha and Bhukia areas.

of mineral development can be recognized. In Ghagri area, the early stage of distal K-Na-Ca-Mg- Fe alteration is manifested in K-feldspar, magnetite, dolomite, ankerite, Na-reibeckite, and minor albite. The late stage Na-Ca-B-K-Mg-Fe alteration is shown by the development of albite, calcite, tourmaline, chlorite, biotite, hematite, phlogopite, and spadaite. At Dugocha, Na-B alteration represented by albite, tourmaline, and graphite is dominant in the early stage, while K-alteration represented by coarse grained granoblastic aggregates of microcline and untwinned microcline zones occurs in later stage. Biotite, chlorite, and hematite are minor minerals during early stage of alteration, whereas they are an important constituent of the late phase alteration. In the Bhukia area the major Na-Ca-Mg-Fe-B-Ti alteration, pervasive in both early and late phases, is manifested by the development of albite, calcite, actinolite, hematite, tourmaline, chlorite, and titanite. K-feldspar alteration is minor. The sulfide minerals associated with early phases include massive, semi-massive, and disseminated pyrrhotite,

and minor amounts of arsenopyrite and chalcopyrite in all the three deposits, though the relative abundance of chalcopyrite and pyrrhotite differ significantly. These three minerals, with dominance of arsenopyrite, continued into the next phase. The late phase sulfide mineralogy significantly differs in Ghagri from that of Dugocha and Bhukia areas. In Ghagri areas pentlandite is observed along the granoblastic margins of the pyrrhotite. In Dugocha and Bhukia areas, beside presence of pyrite, cubanite, bornite, loellingite and Bi-Te and Bi-bearing mineral phases are significant. Gold apparently developed during the late sulfide phase mineralization. Important among the late phase alterations are martitization and pseudomorphic development of hematite over magnetite, development of ankeritic carbonate, late proliferation of calcite veins and development of hydroxide minerals like spadaite and brucite. These observations suggest evolution of the mineral fluids of Salumber-Ghatol belt from much reduced to fairly oxidized environment.

FLUID INCLUSION STUDIES

Dugocha Area: Fluid inclusion studies were carried out on four borehole samples that were collected from a massive to semi-massive auriferous sulfide zone and one from the intervening barren zones from central Dugocha block. All the inclusions were hosted in quartz and, as per their host affiliations, they are referred as mineralized quartz and barren quartz. Petrographically inclusions from both types of quartz are similar. These are represented by Type-1 (monophase) and Type-2 (biphase – L + V) inclusions. Paragenetically, the inclusions could be classified as primary inclusions (isolated, randomly oriented, sub-rounded to irregular shape, large size between 5-20 μm, (Fig.13) and secondary inclusions (occur in arrays, oriented, faceted, elongated, stretched, small size of < 5 microns, (Fig.13). Necking down of primary Type-2 inclusions giving rise to pseudo-secondary inclusions is also noticed. The samples studied indicate that the area occupied by the CO_2 vapour phase range from 1 to 39% (average 8%) and the aqueous phase varies from 61 to 99% with an average of 92%. The CO_2 vapour, whenever present, is perfectly spherical, whereas the CO_2 liquid-aqueous-liquid interface varies from rounded to elliptical and oval. Microthermometric distinction among the Type-2 inclusions, between low saline (Type-2a) and moderate to high saline inclusions could be made (Type-2b). Observed and calculated (calculations made using Linksys software version 1.8 following the equations of state given by Bodnar,1983; Zhang and Frantz, 1987; Brown and Lamb, 1988) microthermometric data of the fluid inclusions are given in Table 8. Inclusions showing (i) apparent necking down; (ii) extremely fine size inclusions; (iii) those occurring in clusters that make distinction between the adjacent inclusions difficult; and (iv) those with highly variable liquid/vapor ratios are excluded from analyses. Therefore a large number of secondary inclusions could not be included in the analytical results.

Microthermometric data of mineralized and barren quartz (Table 8) differ markedly from each other. Temperature of initial melting of ice (T_{im}(ice)) for mineralized quartz range from -58.2 °C to -5.6 °C (average = -35.13 °C), whereas final melting of ice (T_{fm}(ice)) ranges from -34.70 °C to 1.5 °C (average = -15.02 °C). The T_{im}(ice) for barren quartz ranges from -44.9 °C to -17 °C (average = -33.64 °C and T_{fm}(ice) from -15 °C to -0.7 °C (average = -5.89°C). The average T_{fm}(ice) values of both types of inclusions is well below -20.8 °C, so the presence of additional salt is implied (cf. Roedder, 1984; Kreuzer, 2005). The maximum of T_{im}(ice) of -58.2°C may indicate the presence of $CaCl_2$ along with NaCl and H_2O (Shepherd et al. 1985). Presence of metastable ice or clathrates in 3 out of 48 inclusions studied and in 2 out of 48 inclusions studied is also identified by the software. The salinity for the mineralized quartz is much higher (range = 6.52 NaCl wt.% eq to 26.75 NaCl wt. % eq.; mean = 19.39 NaCl wt.% eq.) than those for the barren quartz (range 1.16 NaCl wt.% eq. to 12.85 NaCl wt.% eq; mean = 7.27 NaCl wt.% eq.). Salinity of above 26 NaCl wt.% eq. is well corroborated with the recorded daughter halite crystals in the samples. The temperature of homogenization for primary and secondary fluid inclusions in mineralized quartz and those of primary fluid inclusions in quartz from barren zones are 140.8 °C, 166.8 °C and 164.2 °C respectively. The temperature of homogenization - salinity plot (Fig. 14) for the inclusions studied suggests broad trend at a narrow range of homogenization temperatures. The data could be classified into three groups (i) low salinity barren quartz; (ii) moderate to high salinity of primary phase in mineralized quartzites; (iii) and the high salinity of secondary inclusions in mineralized quartz. The latter data fall proximal to the halite saturation curve. The trend of both primary and secondary inclusions plots from the mineralized quartzites indicates isothermal mixing with fluids of contrasting salinity (Shepherd et al. 1985):

Bhukia area: Previous studies on fluid inclusions of the Salumber-Ghatol region were concentrated exclusively in Bhukia area (Gharia et al. 2001; Guha, 2004; Deol et al. 2008). These studies conducted on different parts of Bhukia gold deposits identify, (i) four types of fluid inclusions in

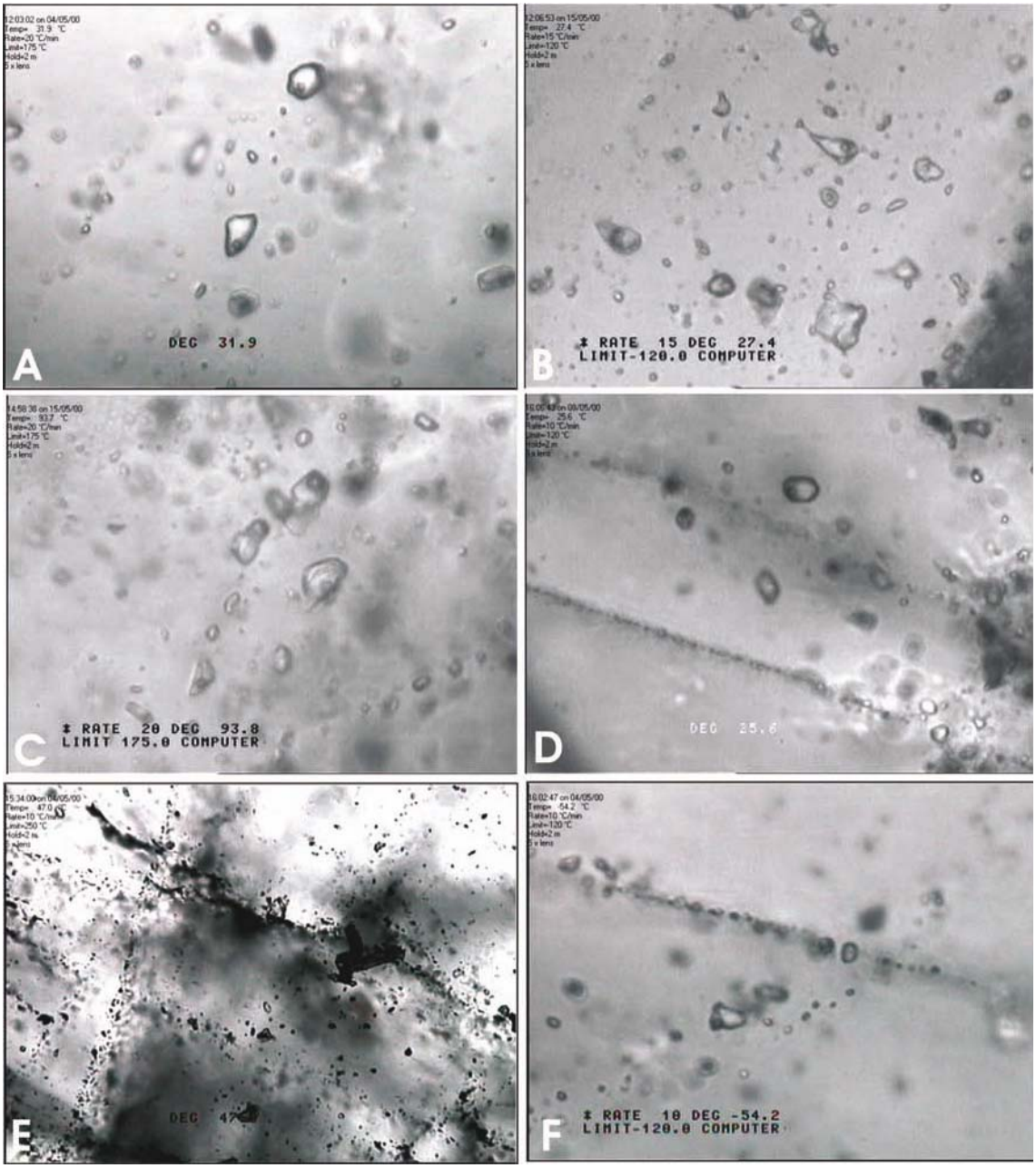

Fig. 13 A. Primary and secondary bi-phase fluid inclusions. Note secondary inclusions along the healed fractures towards northwestern quarter of the image. **B**. Primary two phase fluid inclusions and many secondary inclusions of insignificant size along healed fractures; **C**. Primary and secondary fluid inclusions of different sizes and shapes; **D**. Primary two phase inclusions of different shapes and sizes with variation in different volumes of CO_2 (vapour phase) and small size secondary inclusions along the parallel fractures; **E**. Two sets of healed fractures with an array of secondary bi-phase fluid inclusions with small vapor (CO_2) bubbles; **F**. Two sets of healed fractures with primary and secondary two phase inclusions. Primary two phase inclusions showing different size and shape.

terms of (a) monophase (H_2O vapour phase or a very low density gas), (b) two phase (non-aqueous carbonic, filled with a low-density methane), (c) two phase (aqueous saline but under saturated), and (d) inclusions with daughter minerals and halite crystals; (ii) Based on the microthermometric data fluid composition of H_2O-NaCl-KCl-$CaCl_2$ ($\pm MgCl_2$) (Gharia et al. 2001) and H_2O-NaCl-$MgCl_2$-KCl-$FeCl_2$ (Deol et al. 2008) was inferred; (iii) Deol et al. (2008) reported the T_{fm}(ice) that range from -27.5 to -0.2° C (clustering at -27.5 to -17.6 °C) indicating that the

Table 8. Fluid inclusions thermometric, salinity and density data for Dugocha area

Inclusion No.	Melting of ice °C Initial	Final	Th_{CO_2}	Th_{Total}	Salinity	Density
Primary - Mineralized Quartz						
1	-25.7	-9.7	-56	100.6	13.62	1.05
2	-27.1	-13.4	-56.6	147.8	17.25	1.05
3	-37.8	-23.2	-56.2	129.8	24.41	1.12
4	-34.5	-18.3	-55.8	105.8	21.16	1.11
5	-41.1	-21.1	-52.5	102.6	23.08	1.13
6	-37.3	-25.1	-53.5	152.2	25.53	1.11
7	-51.2	-11.8	-42.3	128.2	15.76	1.05
8	-47.6	-13.2	-54.2	144.7	17.07	1.05
9	-12	-18	-48.6	124	20.95	1.09
10	-42	-18	-48	166.6	20.95	1.06
11	-40.1	-14.5	-56	131.2	18.2	1.07
12	-44.2	-20.1	-56.6	143.9	22.42	1.09
13	-41.8	-18.2	-52.3	122.1	21.09	1.09
14	-33.7	-10.4	-54.9	109.8	14.36	1.05
15	-32.5	-27.3	-25.4	169.1	26.75	1.1
16	-8.5	-2.4	-52	181		0.89
17	-35	-6	-47	154	9.19	0.98
18	-58.2	-13.2		138.1	17.07	1.05
19	-46.3	-37.4		146		0.93
20		-22.1	-50.2	196	23.72	1.06
21	-5.6	1.5	-52	196		0.87
22	-10	2.4	-58	156		0.92
23	-25.6	-12.3	-31.4	166	16.24	1.02
24	-32.4	-23.1	-46.1	172	24.34	1.08
25	-32.5	-18	-39.8	153.5	20.95	1.07
26	-27.3	-10.2	-31.4	131	14.16	1.04
27	-39.2	-4.1	-43.5	127.7	6.52	0.99
28	-33.2	-11.7	-52.1	163.9	15.67	1.02
29	-45.8	-26.3	-53.7	89.4	26.21	1.16
30	-42.2	-20.2	-27.4	81.3	22.69	1.14
31		-22.5	-37.3	130.9	23.98	1.11
32	-41.2	-11.3	-46.8	184.6	15.28	0.998
33	-44.1	-10.4	-50.9	91.8	21.24	1.12
34	-44	-23.2	-48.3	115.4	24.41	1.13
35		-11.3	-48.5	139.7	15.28	1.04
36	-44.2	-16	-50	145	19.43	1.06
37	-41.8	-18	-48.5	173.2	20.95	1.05
Avg.	**-35.4618**	**-15.6243**	**-48.1086**	**140.8351**	**19.39182**	**1.052649**
Secondary - Mineralized Quartz						
37	-42.1	-18.2	-48	166.8	20.95	1.06
38	-41.8	-18.1	-48.1	166.6	20.7	1.05
39	-42.4	18.4	48.2	167.2	21	1.07
Avg.	**-42.1**	**-5.96667**	**-15.9667**	**166.8667**	**20.88333**	**1.06**
Barren Quartz						
1	-44.9	-0.9	-56.6	126.3	1.49	0.95
2	-35.6	-0.7	-56.6	135.1	1.16	0.94
3	-40.2	-7.3	-55.3	136.1	10.85	1.01
4	-32.5	-6.8	-56.6	160.6	10.23	0.98
5	-39.8	-3.2	-56.6	188.2	5.17	0.92
6	-17	-9	-56.5	217	12.85	0.95
7	-25	-15	-60	215	8.62	0.99
8	-35.57	-6.13	-40.74	168.61	8.68	0.96
9	-32.2	-4	-49	131	6.37	0.98
Avg.	**-33.6411**	**-5.89222**	**-54.2156**	**164.2122**	**7.268889**	**0.964444**

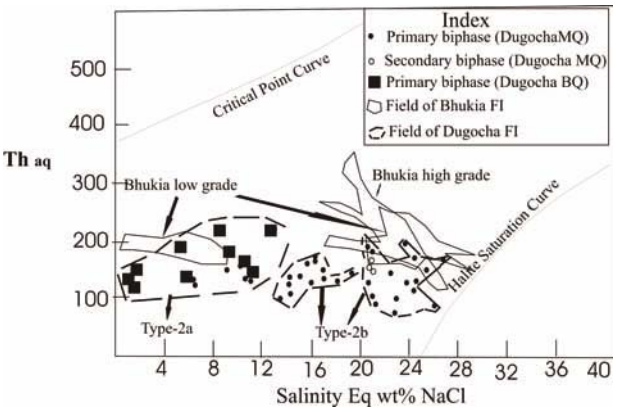

Fig. 14. Salinity (eq. wt. %) NaCl vs Th aq plot for the fluid inclusions from mineral deposits of Salumber-Ghatol belt. Fields of Bhukia fluid inclusions are from Deol et al. (2008).

salinity of the fluid was between 30.07 to 14.87 eq. wt.% NaCl (clustering at 26.86 to 22.35 eq wt. %); (iv) two clusters of contrasting salinity in one sample, one with high salinity 29.14 to 20.65 eq. wt.%) and the other with low salinity (9.05 to 0.33 eq. wt %) at similar Th values suggesting the possibility of mixing of fluids of contrasting salinity. The Bhukia data in Th vs Salinity diagram (Fig.14) suggest two clusters for low and high salinity inclusion from the low grade ore and one cluster proximal to the halite saturation curve for the high grade ore. Interestingly the fluid inclusion cluster for the barren quartz of Dugocha area broadly overlap with the field of low grade gold of Bhukia area and those of mineralized quartz from Dugocha area are proximal to the field of high salinity fluid inclusions of Bhukia area.

Sulfur Isotope Studies

In view of the dominant minerals being pyrrhotite and arsenopyrite in samples, pure fractions of these minerals were separated and selected for sulfur isotopic analysis. The $\delta^{34}S$ values determined for sulfides from Ghagri, Dugocha, and Bhukia deposits are given in Table 9 and plotted in Fig.15. The average $\delta^{34}S$ for the Ghagri pyrrhotite is 11.4 per mil and for the arsenopyrite is 14.5 per mil. As indicated in the ore-mineragraphic studies, the gold bearing arsenopyrite is a dominant phase in the second phase of mineralization in the rock and therefore could be interpreted that the late phase sulphides have much heavier isotopic values than the earlier phase sulphides. The only sulfide phase analyzed in Dugocha prospect is pyrrhotite whose average $\delta^{34}S$ values (11.2 per mil) broadly tally with the values of the pyrrhotite from Ghagri sulfide deposit. The average $\delta^{34}S$ values for pyrrhotite from Bhukia-1 area is 11.6 per mil and for the arsenopyrite is 12.25 per mil which

Table 9. Sulphur isotopic values in sulphide deposits of Salumber-Ghatol belt

Sl. No.	Sample No.	Mineral	δ^{34} S in ‰
Ghagri Area			
1	Gh-1	Pyrrhotite	10.5
2	Gh-2	Pyrrhotite	10.4
3	Gh-3	Pyrrhotite	10.3
4	Gh-4	Pyrrhotite	14.4
Average for pyrrhotite			11.4
5	Gh-5	Arsenopyrite	13.7
6	Gh-6	Arsenopyrite	13.9
7	Gh-7	Arsenopyrite	16
Average for arsenopyrite			14.53
Dugocha Area			
8	F-30	Pyrrhotite	10.5
9	F-52	Pyrrhotite	10.6
10	DCH-4	Pyrrhotite	10.4
11	DCH-6	Pyrrhotite	15.6
12	DCH-1	Pyrrhotite	11.1
13	DCH-2	Pyrrhotite	10.17
14	DCH-3	Pyrrhotite	10.08
Average for Dugocha Pyrrhotite			11.20
Bhukia Area			
Bhukia - 1			
15	18/16	Pyrrhotite	11.8
16	27/68	Pyrrhotite	11.4
Average for pyrrhotite			11.6
17	27/5	Arsenopyrite	11.9
18	18/159	Arsenopyrite	11.6
19	18/162	Arsenopyrite	11.7
20	27/68	Arsenopyrite	13.8
Average for arsenopyrite			12.25
Bhukia - 2*			
21	18/17	Pyrrhotite	12.8
22	27/67	Pyrrhotite	13.7
23	18/32	Pyrrhotite	14.98
24	18/16	Pyrrhotite	13.93
28	27/68	Pyrrhotite	13.46
Average for pyrrhotite			13.774
25	18/159	Arsenopyrite	13.74
26	18/62	Arsenopyrite	13.89
27	27/16	Arsenopyrite	16.01
29	18/208	Arsenopyrite	13.02
30	27/5	Arsenopyrite	13.95
Average for arsenopyrite			14.12

* Data from Golani et al., 2002

tallies well with the early phase sulphides of the Ghagri and Dogocha areas. Distinctly heavier isotopic values are recorded for the Bhukia-2 (δ^{34}S = 13.77 and 14.12 per mil respectively for pyrrhotite and arsenopyrite). The sulphur isotopic signatures from the three deposits could be interpreted in terms of (i) the late sulphide mineral phases possess comparatively heavier isotopic values (ii) the narrow range of δ^{34}S implies that despite local disequilibrium between the two phases of mineralization within individual

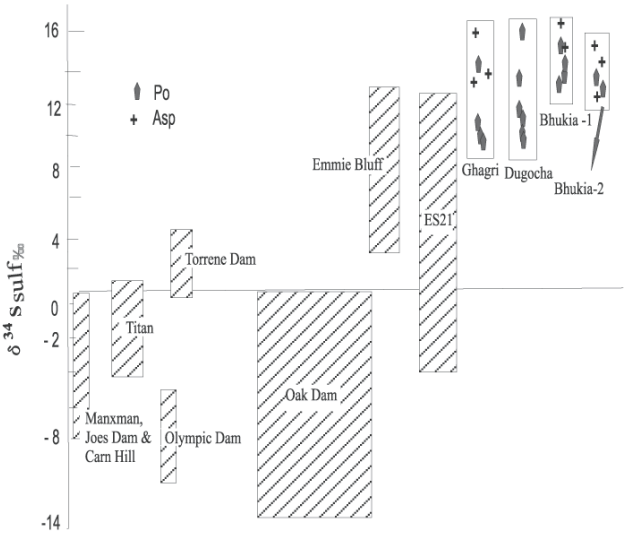

Fig.15. δ^{34}S plots for the sulfides from mineral deposits of Salumber-Ghatol belt. The fields for IOCG-type mineral deposits of Manxman, Joes Dam, Carn Hill, Olympic Dam, Titan, Torrene Dam, Oak Dam, Emmie Bluff are from Bastrakov et al. (2007) and for Bhukia1 and Bhukia 2 see Table 9.

deposit, the source of δ^{34}S for all the three deposit is same (iii) significantly higher positive δ^{34}S values of ~10 to ~15 per mil clearly rule out the possibility of either magmatic (generally δ^{34}S values of -5 to + 5 permil, Neilsen et al. 1979) or biogenic (> 20 per mil, Neilsen, 1979) source for sulfur and (iv) the moderately high δ^{34}S values therefore suggest metasedimentary source for sulfur (Nielsen, 1979). The data for these deposits match well with those of Emmie Bluff IOCG deposit of Gawlar Craton (Fig. 15). The Emmie Bluff deposit is interpreted to have metasedimentary rock source or sea water or evaporitic water source (Bastrakov et al. 2007).

Iron Mineralization

Notwithstanding frequent references to iron oxide concentrations in Cu-Au ore zones and ancient workings presumably for iron in the region (Basu et al. 1968; Iqbaluddin and Bhattacharya, 1971; Bhattacharya et al. 1995; Ghariya et al. 1998), there is no systematic study of iron mineralization in Salumber Ghatol belt. Besides the occurrence of magnetite bearing feldspathic rocks in Ghagri area (Fig.8I) that sometimes constitute conspicuous layers (Fig. 11K) and locally becomes thick bands, the Fe-oxide concentrations occur in three other settings in Salumber-Ghatol belt. These are (i) as magnetite disseminations in excess of 15 volume % in albite-dolomite-magnetite rocks; (ii) as veins and disseminations of specular hematite within albitites and (iii) as ferruginous quartzite bands at some

localities like Matasula and Manpura. The albite-dolomite-magnetite rocks of Ghagri area analyse between 12.45 wt % and 25.67 wt% of Fe_2O_3 (Table 10A). With virtual absence of any other ferromagnesian minerals in the rock, bulk of the Fe_2O_3 analyzed represent the concentration of the magnetite grains in the rock. The magnetites in these units are intimately associated with sulphides (Fig.8K). Microprobe data (Table 5) suggests that these are essentially low titanium magnetites or maghemites. About 3.5 km NE of Boraj bands of albite-hematite and albite-specular hematite breccia having width ranging in thickness from 2 m to 5 m occur within granite gneiss. Specular hematite is also an important constituent of ferruginous quartzites of Beras area (24°13'30";74°07'). Two bed rock grab samples of this rock analysed 0.1 wt % and 3.0 wt% of Cu. Bedawal and Kalipole area (24°09'10"; 74°13'40") contain cupriferous specular hematite quartzite bands that are characterized by malachite stains, streaks, lenses, stringers and fine laminae of chalcopyrites. Cu contents of six grab samples range between 0.12 wt% and 1.4 wt%. In Manpura area ferruginous quartzites are represented by hematite-quartz breccia (Fig. 8L). In Mata Sula area 10-20 m thick

Table 10A. Major element geochemistry of altered rocks from Salumber-Ghatol belt

	Ghagri area																		
	Microclinites									Albite Microcline Rock					Albite-magnetite-dolomite rock				
	1	2	3	4	5	6	7	8	9	10	11	12	13	14	15	16	17	18	19
Samp No.	6/F-	7/F	10/F	11/F	12/F	13/F	14/F	GH/1/ 1*	GH/2/ 2*	8/F- 7GR	9/F	GH- 3*	GH- 4*	GH/2/ 1*	SG-5	RGH 2/ 4	RGH 4/ 1	RGH5/ 3	3/ GR02
XRF No.	19326	19331	20934	20940	22557	22560	20143	20142	20139	19332	19334	20144	20145	20138	22558	2-141	20942	20933	19328
SiO_2	62.5	49.87	58.17	65.19	61.4	52.37	59.94	61.09	57.72	54.04	55.46	57.85	56.23	61.58	44.55	48.33	44.15	39.62	40.08
TiO_2	0.13	0.98	1.01	0.89	0.62	0.76	0.97	0.77	1.06	1.34	0.81	1.06	1.07	1.01	2.34	2.7	1.63	1.72	2.2
Al_2O_3	17.8	14.07	12.73	11.72	11.6.9	11.68	11.38	11.8	11.3	13.74	12.54	13.68	14.23	11.62	6.81	11.64	11.27	9.16	10.71
Fe_2O_3	3.02	13.25	7.6	5.71	5.27	7.86	7.22	5.85	10.13	14.78	13.39	11.03	12.45	6.38	19.97	21.52	15.09	12.45	20.95
MnO	0.02	0.28	0.49	0.43	0.27	0.36	0.29	0.26	0.19	0.4	0.24	0.04	0.03	0.25	0.48	0.22	0.51	0.95	0.6
MgO	0.21	1.36	1.87	1.2	3.73	4.85	2.58	2.35	1.67	0.56	0.42	3.52	2.58	2.21	3.81	2.07	6.58	7.03	2.2
CaO	0.06	2.96	2.65	2.25	4.3	5.68	4.3	4.26	2.8	1.51	2.6	0.33	0.35	3.49	6.56	2.46	5.14	9.17	6.33
Na_2O	0.45	0.4	0.36	0.01	0.56	0.63	0.42	0.25	0.1	2.2	0.63	3.1	2.8	4.77	6.66	5.32	6.51	4.54	5.89
K_2O	15.35	12.8	10.78	9.35	9.24	8.34	9.77	9.42	10.3	9.39	11.08	7.88	8.96	2.8	0.18	1.86	1.13	0.89	1.03
P_2O_5	0.01	0.1	0.16	0.14	0.09	0.08	0.1	0.07	0.08	0.13	0.09	0.11	0.15	0.09	0.32	0.42	0.24	0.16	0.27
S	0.01	0.01	0.64	0.31	0.12	0.13	bld	bld	bld	0.02	0.02	bld	bld	bld	0.18	bld	0.14	0.67	0.02
Cr_2O_3	bld	0.03	bld	bld	bld	bld	0.03	0.04	0.03	0.05	0.03	0.03	0.03	0.09	bld	bld	0.11	0.04	bld
NiO	bld	bld	0.01	bld	bld	0.01	bld	bld	bld	bld	0.01	0.02	0.01	bld	bld	bld	0.01	0.01	bld
BaO	0.1	0.01	0.04	0.02	0.02	0.02	bld	bld	bld	0.01	0.02	0.01	bld	bld	bld	bld	0.02	0.01	0.01
LOI	0.22	3.72	3.48	2.65	3.68	3.27	2.22	3.03	4.13	1.94	2.82	0.58	0.33	5.07	9.12	2.63	6.44	13.38	8.21
Total	**99.88**	**99.84**	**99.99**	**99.87**	**99.99**	**99.98**	**99.22**	**99.21**	**99.51**	**100.11**	**100.16**	**99.24**	**99.22**	**99.36**	**99.98**	**99.17**	**98.97**	**99.8**	98.5
Na_2O/K_2O	0.03	0.03	0.03	0.00	0.06	0.08	0.04	0.03	0.01	0.23	0.06	0.39	0.31	1.70	37.00	2.86	5.76	5.10	5.72

	Ghagri area				Dugocha Area								Bhukia Area				Mata Sula area	
	Albite-magnetite-dolomite rock				Albitite			Albite-Microcline rock		Albite-Dolomite-Magnetite rock			Albitite	Albite-microcline rock		Alb. amph.	Magnetite quartzite	
	20	21	22	23	24	25	26	27	28	29	30	31	32	33	34	35	36	37
Samp No.	4/ GR02	5/ GR02	8/ GR02	RG4/ 35	16/F- C-1	17/F- C-2	20/F- F39	18/F- F17	19/F- F-23	FD-03	DGH W-2	F-4	DB/2/ 10	FD-B/ 1/6	FD-B2/ 10	BK-5	MTS -1	MTS -2
XRF No.	19329	19330	19333	20943	24866	24867	18687	18683	18680	24272	24477	24474	18500	18499	18498	25345	25346	25347
SiO_2	43.89	34.23	31.41	43.57	59.7	59.77	52.24	56.78	54.86	4.04	4.73	2.38	57.86	55.25	61.08	63.22	54.7	48.97
TiO_2	1.42	1.3	1.67	1.23	0.68	0.8	0.8	1.3	0.62	bld	bld	bld	0.97	1.43	1.1	0.31	0.04	0.01
Al_2O_3	11.32	8.19	8.71	11.41	15.93	16.42	15.22	20.1	18.34	bld	bld	bld	9.11	12.41	15.11	9.36	2.04	0.89
Fe_2O_3	21.31	18.73	25.67	15.27	0.09	2.51	8.05	4.31	1.71	15.53	24.84	21.9	9.56	7.04	4.98	8.61	37.75	44.09
MnO	0.4	1.31	0.93	0.35	0.01	0.83	0.02	0.02	0.01	1.02	1.14	1.85	0.22	0.09	0.09	0.64	0.16	0.25
MgO	4.69	4.21	2.96	10.55	0.12	0.89	bld	1.81	1.74	bld	bld	bld	5.47	2.48	1.85	5.05	1.28	1.79
CaO	4.63	10.6	10.37	5.46	1.46	3.02	1.14	0.14	1.25	35.05	28.82	31.99	5.35	4.44	3.89	5.64	3.04	1.87
Na_2O	4.91	4.54	4.69	4.01	11.08	7.34	8.52	2.4	3.48	2.38	bld	0.87	7.33	6.64	5.2	4.14	<0.1	<.01
K_2O	1.33	0.79	1.23	3.79	0.61	0.61	0.4	5.63	6.05	bld	bld	bld	0.53	7.59	4.33	0.31	0.11	0.01
P_2O_5	0.17	0.22	0.3	0.11	0.03	0.08	0.08	0.06	0.05	0.33	0.27	0.13	0.08	0.1	0.04	0.07	0.36	0.29
S	0.02	0.04	0.04	0.21	0.96	1.28	0.09	0.02	0.35	2.04	2.76	1.99	0.19	0.09	0.16	0.15	0.26	0.31
Cr_2O_3	bld	bld	0.01	bld	0.01	0.02	bld	0.01	0.01	bld	bld	bld	0.13	0.11	0.03	0.02	0.01	<.01
NiO	bld	bld	bld	0.01	bld	0.02	0.03	0	bld	0.02	0.01	0.01	0.02	0.02	0.01	<.01	<.01	<.01
BaO	0.03	bld	bld	0.03	0.02	0.02	2.34	0	0.08	0.11	0.1	0.11	bld	bld	bld	79*	160*	310*
LOI	4.3	14.88	10.95	3.94	10.42	5.32	11.16	7.12	6.45	39.47	37.32	38.75	1.23	1.87	1.4	0.66	0.95	0.98
Total	**98.42**	**99.04**	**98.94**	**99.94**	**101.12**	**98.93**	**100.08**	**99.7**	**95.02**	**99.99**	**99.99**	**99.98**	**98.05**	**99.56**	**99.27**	**98.18**	**100.7**	**99.46**
Na_2O/K_2O	3.69	5.75	3.81	1.06	18.16	12.03	21.30	0.43	0.58	13.83	0.87	1.2	13.35					

Table 10B. Trace element composition of altered rocks from Salumber-Ghatol belt

	Ghagri Area												Dugocha Area				
	Microclinites								Albite Microcline Rock				Albitites		Albite-Microcline Rock		
	1	2	3	4	5	6	7	8	9	10	11	12	13	14	15	16	17
Sr	950.00	110.00	170.00	125.00	152.00	145.00	165.00	120.00	165.00				80.00	80.00	140.00	150.00	50.00
Ba	20.00	20.00	20.00	20.00	40.00	50.00	40.00	20.00	20.00				85.00	110.00	85.00	440.00	910.00
Ta	1.80	1.60	1.60	1.70	1.00	1.40	1.20	1.00	1.00				0.80	0.90	0.80	1.20	1.30
Be	<0.3	0.40	<0.3	<0.3	<0.3	<0.3	<0.3	0.31	0.32				0.62	1.47	2.65	3.38	0.33
Ga	15.85	16.26	13.44	12.85	10.96	11.01	11.47	16.95	13.94				20.11	27.51	21.16	31.89	35.51
Ge	1.21	1.49	1.05	1.32	1.78	1.48	1.59	1.51	2.00				1.45	1.81	2.05	2.31	1.79
As	<2	<2	7.66	26.31	3.58	10.10	<2	21.78	<2				142.36	635.06	34877.70	14.46	40.37
Y	1.93	32.75	22.44	21.00	16.36	14.97	15.28	16.80	11.83				15.35	20.63	17.15	43.72	32.37
Zr	7.87	138.97	114.28	99.43	66.61	125.32	92.85	154.52	110.60				118.72	133.80	111.56	257.55	152.64
Nb	2.48	8.89	7.28	3.53	3.33	3.82	5.98	7.91	7.63				12.04	16.79	12.53	23.03	12.20
Cs	1.82	1.43	0.68	0.53	0.78	0.47	4.33	0.41	3.18				0.42	1.43	0.24	4.19	0.41
Hf	<0.2	3.78	3.06	2.64	6.61	3.26	2.53	4.15	3.07				3.48	3.89	3.39	7.46	4.26
Bi	<0.1	0.26	<0.1	0.75	<0.1	<0.1	<0.1	0.10	0.30				<0.1	8.22	18.32	0.86	0.25
Th	0.23	8.77	3.99	3.99	3.37	2.96	3.99	5.31	5.53				13.51	9.24	18.10	19.11	15.93
U	<0.5	4.19	1.24	2.68	1.30	1.51	1.47	1.34	2.78				3.30	6.52	11.50	5.72	6.90
La	1.32	45.79	28.35	28.42	19.52	12.99	16.39	19.53	29.09	20.00	22.00	21.00	34.14	129.93	128.99	33.91	140.97
Ce	2.71	68.91	41.23	47.87	35.72	25.67	32.15	39.10	42.31	40.00	40.00	35.00	75.41	239.91	266.33	53.31	254.78
Pr	0.30	9.41	5.62	6.48	4.53	3.23	3.97	4.86	5.63				9.90	28.67	34.75	6.97	30.68
Nd	1.21	32.73	20.90	24.36	17.30	12.54	15.22	18.61	19.83	17.00	16.00	15.00	37.14	105.70	129.12	25.85	109.95
Eu	0.28	1.43	1.41	1.37	1.07	0.88	0.97	1.21	0.93	1.20	1.20	1.00	0.92	2.73	2.44	1.21	2.45
Sm	0.74	5.80	4.26	4.71	3.46	2.60	3.09	3.90	3.79	3.60	3.50	3.50	6.25	17.29	20.88	5.18	18.13
Tb	0.06	0.86	0.65	0.66	0.51	0.42	0.47	0.53	0.43	0.65	0.62	0.60	0.60	1.37	1.41	0.94	1.57
Gd	0.36	5.13	3.95	4.24	3.25	2.59	2.87	3.37	2.98				4.32	12.23	13.42	5.17	12.99
Dy	0.37	5.21	3.82	3.64	2.77	2.49	2.62	2.93	2.28				2.96	5.10	4.71	6.28	6.79
Ho	0.07	1.14	0.78	0.74	0.56	0.53	0.53	0.59	0.43				0.56	0.76	0.66	1.39	1.20
Er	0.16	2.95	2.04	1.82	1.39	1.37	1.37	1.57	1.06				1.34	1.67	1.50	3.76	2.85
Tm	0.03	0.48	0.32	0.31	0.23	0.23	0.22	0.27	0.17				0.22	0.26	0.24	0.65	0.45
Yb	0.17	2.81	1.94	1.82	1.38	1.40	1.39	1.71	1.15	1.30	1.00	1.40	1.28	1.62	1.65	4.06	2.81
Lu	0.03	0.40	0.28	0.26	0.21	0.20	0.22	0.27	0.18	0.13	0.10	0.20	0.18	0.26	0.27	0.60	0.41

bands of banded magnetite-quartzite occur. The magnetite quartzites of this area are intensely mylonitized with alternation of deformed and stretched quartz (with minor dolomite) and magnetite/maghemite. Ore microscopic studies suggest that the magnetite are euhedral to subhedral arranged in irregular layers and invariably show recrystallised texture with well defined triple points. Martitisation with fairly well developed hematite patches (Fig. 8K) could be seen in the magnetite grains. The whole-rock analyses of these banded magnetite quartzites (Table 6) indicate ~ 38 wt % to 44 wt % Fe_2O_3 . Though Basu et al. (1968) contended that such zones could be exploited economically the resource estimation of these iron-oxide deposits awaits further detailed exploration.

Uranium Mineralization

The altered rocks (albitites and albitic microcline rocks) in Salumber-Ghatol belt show generally elevated levels of uranium and thorium (average ~7 ppm and ~15 ppm respectively, Table 10B). Regional evaluation for the exploration of radioactive elements was recently undertaken by the Atomic Minerals Directorate for Exploration and Research (Chawla et al. 2007). This study resulted in identification of seven priority zones for uranium mineralization. The anomalous radioactive zones coincided with the shear controlled, iron-rich brecciated and catalastic rocks that also host sulfide mineralization in this region. The radioactive rock samples assayed 0.012% to 0.18% U_3O_8 and < 0.005% to 0.023% ThO_2. Thucolite, discrete uraninite cuboids in carbonaceous matter, uraninite with globular carbonaceous matter (graphite) represent uranium mineralization in the cataclasites. Uraninite is in intimate association with sulfides (pyrite, arsenopyrite, pyrrhotite, chalcopyrite, covellite, and bornite). Uranium in iron-rich brecciated/cataclastic set up with deep seated faults/shear in albitized zones confirms uranium potentiality of this region (Chawla et al. 2007).

GEOCHEMISTRY OF ALTERED ROCKS

The petrographic distinction of the two contrasting type of feldspathic rocks in Ghagri and Dugocha is evident from their whole rock chemistry (Table 10A and B). Ghagri rocks are distinctly ultrapotassic (Table 10A average K_2O = 9.67%; average Na_2O/K_2O = 0.215), whereas those from Dugocha-Bhukia are ultrasodic in nature (average Na_2O ~ 7.0%; average Na_2O/K_2O = 13.22). In view of total recrystallization under conditions of lower grade

metamorphism of the unusual constituent mineral phases in altered felsic rocks of both areas, the most important information sought from the chemical data is regarding the igneous or sedimentary parentage of the precursor rocks. The feldspathic rocks, when plotted in MgO vs other major oxides and trace elements diagram (Fig. 16), exhibit systematic decreasing trends for $Fe_2O_3^T$, SiO_2, Zr, Na_2O, and K_2O and increasing trend for CaO and TiO_2. Within/among Ghagri rocks, distinction can be made in terms of distal alteration represented by microclinites and proximal alteration represented by albite-microcline-dolomite-magnetite bearing rocks (AMR and AMDR). The former rocks are ultrapotassic (K_2O > 9 wt.%, up to 15 wt.%; Na_2O/K_2O = 0.001 to 0.07) with moderate levels of $Fe_2O_3^T$ and moderate to high MgO (average = 2.2 wt.%). The latter, on the other hand, are potassic (average K_2O = 8.022 wt.%; Na_2O/K_2O = 0.05 to 1.7), and high in iron with moderately high levels of Na_2O (average = 2.77 wt.%) and MgO (average = 1.85 wt.%). Amongst Dugocha rocks, the graphitic albitites have Na_2O ranging from 7.34 to 11.08 wt.% (average Na_2O = 9.38 wt.%; Na_2O/K_2O ratio = 12 to 21). The albite-microcline rocks (AMR) have significant amount of K_2O (up to 6.28 wt.%; Na_2O/K_2O = 0.43 to 0.57), that often exceed Na_2O content in the rock.

Apart from the abundance of specific alkali elements, the other most illustrative difference in the chemistry of

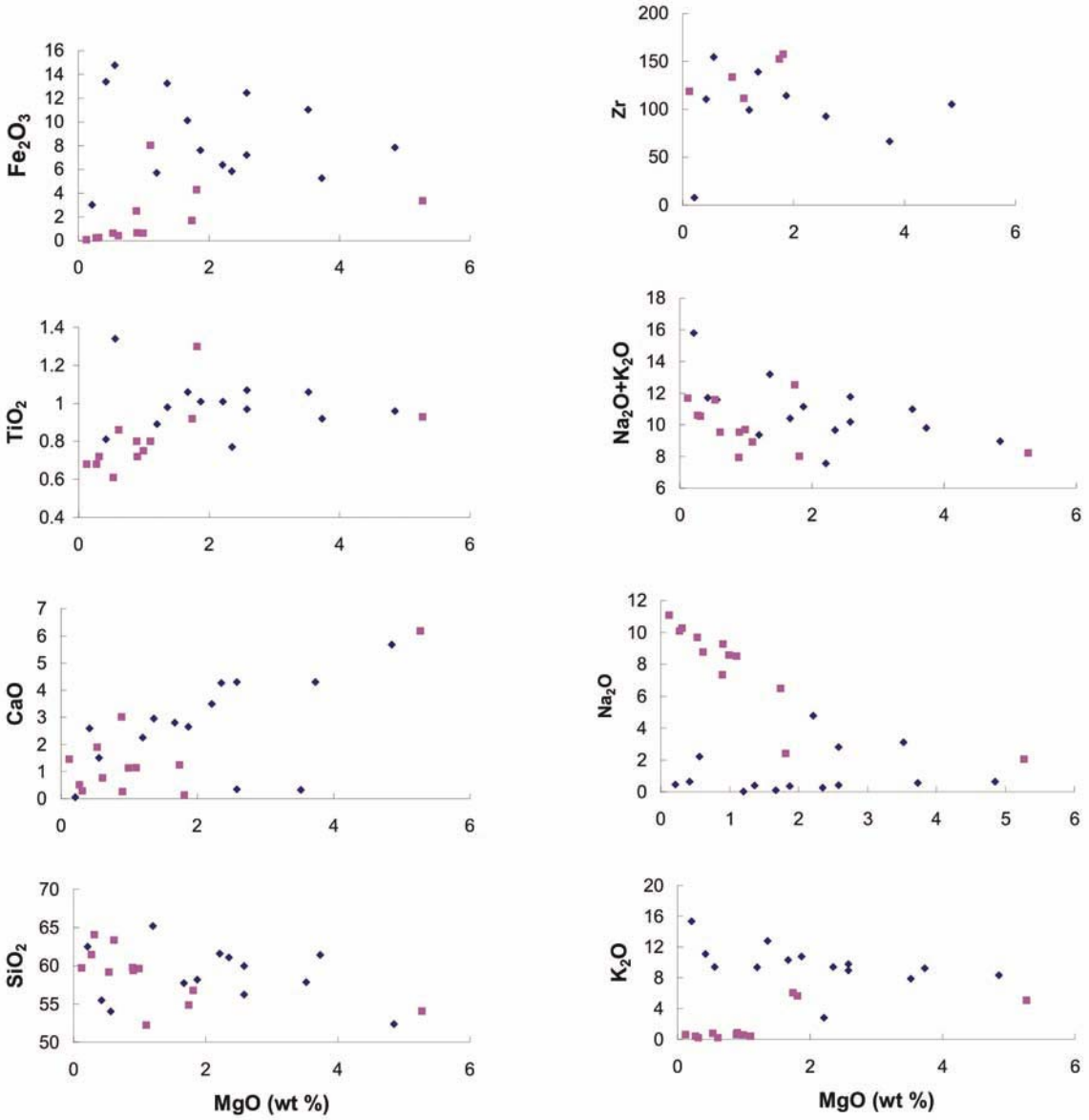

Fig. 16. MgO vs major oxide plots for the feldspathic rocks of Ghagri and Dugocha areas. Symbols used: diamonds = Ghagri microclinites; squares = Dugocha albitites.

feldspathic rocks of the two areas and amongst the rocks of individual areas can be noticed in the absolute abundances of REE. The Ghagri rocks have less REE and least fractionated pattern (Table 10B, Fig.17, $Ce_N/Yb_N = 4.38$). The rock that has analyzed K_2O in excess of 15 wt.% has the least ΣREE and elevated MREE, particularly in the levels of Sm and Eu. The C1 chondrite-normalized REE patterns of the amphibole-bearing microclinites and that of albite-dolomite-bearing microclinites exhibit a negative trough in Sm and Eu region and appears to be a complementary pattern to the pattern of pure microclinites. The ΣREE for Dugocha albitites and AMR are much higher (361 and 447 ppm, respectively) and exhibit much higher degree of fractionation ($Ce_N/Yb_N = 34.18$ and 14.41, respectively). The two variants of the Dugocha area exhibit almost identical REE patterns with enriched LREE, a negative Eu anomaly, and flatter HREE pattern. The only difference between them, however, is higher ΣREE for AMR compared to the albitites. The primitive mantle-normalized, multi-element plot for the different rock types of Ghagri and Dugocha areas is shown in Fig.18. The patterns exhibit depletion in incompatible trace elements like Nb, Sr, P, Zr, and Ti for both suites of rocks. U and Th contents are considerably richer. When their averages are plotted, the similarities between the primitive mantle-normalized patterns of the two suites of rocks become abundantly clear. The difference between the two patterns, just like the C1 chondrite-normalized REE patterns, is in the absolute abundance of the trace elements. The Ghagri samples have much lower absolute abundance of elements compared to Dugocha rocks.

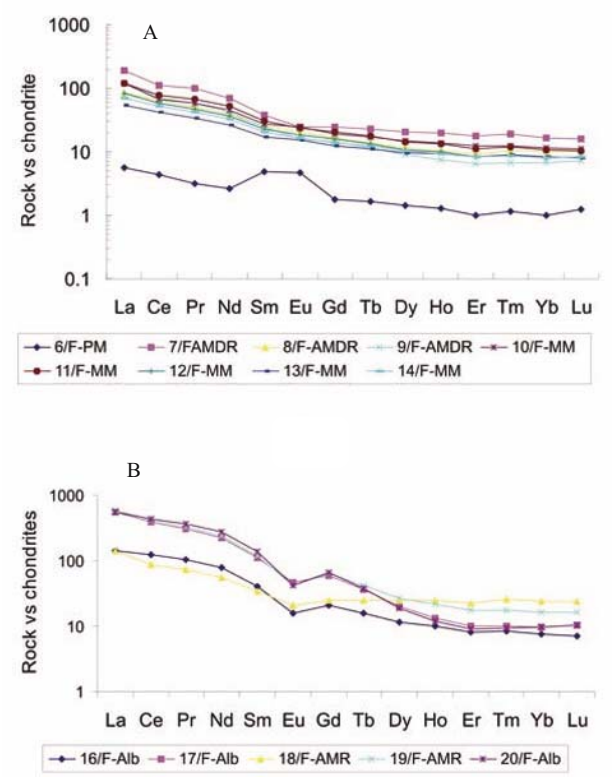

Fig. 17. C1 chondrite-normalized REE patterns for the feldspathic rocks of the study area. **A**. REE pattern for Ghagri feldspathic rocks Abbreviations used with sample numbers are: PM – Pure Microclinites, AMDR – Albite microcline dolomite rock, MM – Magnetite-magnesioriebeckite microclinites. **B**. REE pattern for the Dugocha albitites and syenitic rocks. Abbreviations used with sample numbers are: Alb – Albitites, AMR – Albite microcline rock.

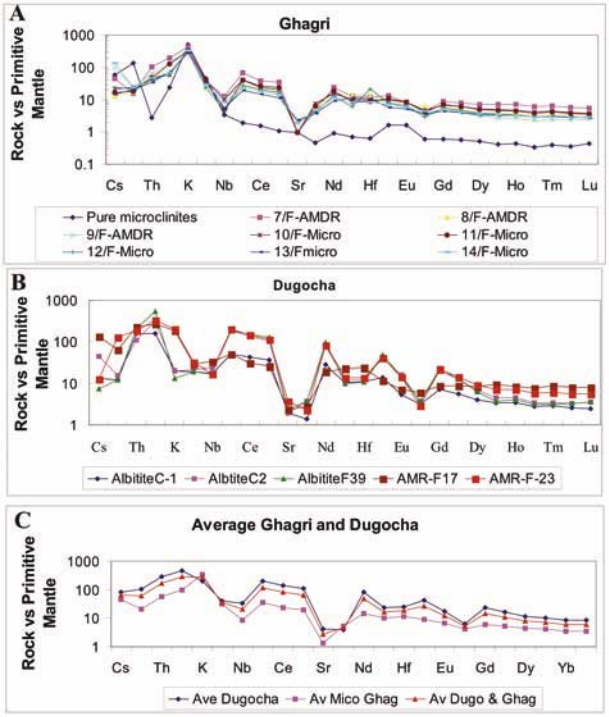

Fig.18. Primitive mantle normalized multi-element plots (normalizing values after Sun and McDonough, 1989) for feldspathic rocks of the study area. **A**. average of Ghagri microclinites; **B**. average of Dugocha albitites and **C**. average of both Ghagri microclinites and Dugocha albitites.

DISCUSSION

The carbonate rocks at Ghagri and at Dugocha-Bhukia areas represent depositions at two stratigraphically distinct horizons, i.e Ghagri in the lower stratigraphic level and Dugocha-Bhukia carbonates at higher stratigraphic levels Debari Group. The Cu-Au mineralization, together with deposit-specific alteration zones are concentrated along the dilational domains in shear zones related to the second deformational event in the area though some studies suggest protracted period of mineralization, the earliest phase being

related to the first phase of the folding event and concomitant shearing (Deol et al. 2008) that continued during the second deformational episode.

The Mg-Fe-Mn-rich dolomite marble at Ghagri display (i) REE signatures of hydrothermally altered marine carbonates and (ii) carbon isotope values that suggest (a) events of decarbonation (depleted isotopic values) and (b) 1.9 Ga old event of positive excursion (cf., Sreenivas et al. 2001). The ultrapotassic alteration zones (> 9 wt% K_2O) and potassic + sodic alterations (~ 10 wt .% $Na_2O + K_2O$) in this deposit are represented by cryptocrystalline Fe-enriched REE-poor, least fractionated magnetite-magnesioriebeckite-microclinites and REE-enriched fractionated albite-microcline rocks. The unusual magnetite-microclinites are rather rare in literature and possibly the nearest analogue may be the magnetite-microcline gneisses reported from the IOCG deposits of eastern United States (cf. Williams et al. 2005). There appears to be distinct host rock influence on the invading hydrothermal fluids as exemplified by (i) the pervasive development of magnesio-reibeckites + phlogopite + spadaite assemblages in ultrapotassic microclinites; the Mg-Na-K bearing mineral assemblages could have been developed by the release of Mg from the dolomitic marble to invading alkali-rich fluids during wall rock alteration and (ii) the development of hybrid rocks like albite-microcline-dolomite rocks.

In striking contrast the Dugocha carbonates are Fe-Mn poor calcitic marbles with highly variable LREE and carbon isotopic values showing pervasive mixing of isotopically distinct carbon. The vein and stringer-type, shear controlled epigenetic sulfide mineralization here develops ultrasodic alteration (>9 wt.% Na_2O) zones manifested in crypto-crystalline albite-graphite-tourmaline rock that shows fractionated REE pattern compared to the rocks of the Ghagri alteration zones. This atypical mineral assemblage contains voluminous graphite that attain up to 8 wt.% or in excess of 20 volume percent. An important observation that is contrary to the alteration zones of Ghagri and Bhukia is the subdued development of Fe-oxide in this assemblage. Williams et al. (2005) have drawn attention towards the existence of IOCG-related Cu-Au deposits localized by carbonaceous metasedimentary rocks in Scandinavia, Cloncurry district and in Khetri, Rajasthan where graphite contributed from ore-fluids and its destruction in favor of carbonate is suggested as a consequence of redox reaction between ore fluids and graphite. The Dugocha graphite contains $\delta^{13}C$ of graphite in excess of -17 ‰ suggesting the carbon to be of organic in nature. It is therefore reasonable to assume that the graphite with biogenic isotopic signatures in this alteration rock could have been contributed from the host metasedimentary units. The heterogeneous mineralized carbonates at Bhukia range from calcitic carbonates to Mg-rich (tremolite bearing) and Mg + Na rich (scapolite and brucite-bearing) dolomite carbonates. The petrographic distinction is also reflected in its stable isotopic composition that show bimodal distribution of $\delta^{13}C$ values near zero per mil that indicate normal marine depositional signatures and much depleted (mean = -3.1 ‰) values.

Deb (2008) has quoted U-Pb zircon ages of albite-rich rock from Bhukia area to range between 1740 and 1820 Ma. The age of Ghagri mineralization is not known, but the age of host dolomites could be constrained indirectly. The age of the basal Delwara volcanic sequence that occurs at the base of Delwara Formation is ~ 2000 Ma (Deb and Thorpe, 2004). The Ghagri dolomite marble occurs between Delwara volcanic rocks (~2000 Ma) and Bhukia feldspathic rock (1740-1820 Ma) and therefore its age should be around 1900-1800 Ma. This assumption is in tandem with the recorded positive carbon isotopic values in the associated carbonates having the global 1.8-1.9 Ga old positive excursion event (cf., Sreenivas et al. 2001). The ages of the host dolomites therefore overlaps between 1.9-1.8 Ga and 1.8-1.7 Ga for Ghagri and Dugocha areas, respectively.

Cu-Au Deposits of Salumber-Ghatol Sector – Are they Similar to IOCG Type Mineralization?

The mesothermal Fe-oxide-Cu-Au-REE-U (Iron-Ore-Copper-Gold type (IOCG)) deposits, include hundreds of occurrences reported from all continents having a variety of tectonic settings from Archaean to Holocene (Meyers, 1988; Hitzman et al. 1992; Barton and Johnson, 1996; Williams et al. 2005). The key features that distinguish these deposits (Williams et al., 2005) are: (i) presence of copper with or without Au as economic metal; (ii) hydrothermal vein breccia and/or replacement ore style, characteristically in specific structural sites; (iii) abundant magnetite and/or hematite, with some districts containing cogenetic deposits in which host rock influence appears to have suppressed the formation of Fe-oxides; (iv) iron-oxides which have low Ti content compared to those in most igneous rocks; (v) absence of clear association with igneous intrusions, such as those characterized by porphyry or skarn deposits and (vi) exceptionally voluminous, generally pervasive alkali metasomatism (mainly sodic alteration and less commonly potassic alterations) and ores enriched in a distinctive, geochemically diverse suite of minor elements including various combinations of F, P, Co, Ni, As, Mo, Ag, Ba, LREE, and U. Besides their spatial distribution (that sometimes spread over hundreds of kilometers, e.g., Andean belt), this

distinct class of deposits contain huge tonnage of gold and other metals (e.g., Gawler Craton contains world's largest resource of gold, copper, and uranium) and physical characteristics that are amenable for geophysical exploration techniques (Skirrow and Davidson, 2007). The diversity of deposits included in the family is such that no single descriptive model can adequately explain the reported features and consequently lacks consensus regarding their mode of origin (Barton and Johnson, 2004; Williams et al. 2005). There are three major explanations provided for the co-existence of albitic alteration with Fe oxide-Cu-Au deposits (Oliver et al. 2004): (1) albitisation occurs as a consequence of hydrothermal fluid circulation around sea floor by hydrothermal cell and inferred to occur in the high temperature portions of such flow systems as a consequence of stability of albite relative to potassic minerals; (2) as the product of recrystallized (diagenetic to metamorphic) evaporitic sediments (Cook and Ashley, 1992) and (3) as crystallization product of fluids released from igneous sources (Hitzman et al. 1992; Oreskes and Einuidi, 1992). In the third case, highly saline fluids are interpreted to have exsolved from crystallizing intermediate or felsic magmas and move down along temperature flow paths and this forms the source for metals and brines.

Distinctive features that the Cu-Au deposits of Salumber-Ghatol sector share with the Proterozoic IOCG deposits are (i) presence of copper with economic quantities of gold; (ii) general elevated levels of uranium in this belt and uranium mineralization in the form of uraninite disseminations in association with sulfides (pyrite, arsenopyrite, pyrrhotite, chalcopyrite, covellite and bornite) in iron rich brecciated/cataclastic rocks (Chawala et al. 2007); (iii) sporadically high cobalt and bismuth in the sulfide zones (this study; Golani et al. 2002; Suresh Chander and Sisodia, 2003); (iv) titanium free magnetite disseminations, (v) structurally controlled, epigenetic mesothermal mineralization; (vi) pervasive sodic and potassic alterations that spreads for 10s to 100s of km^2; (vii) saline mineralizing fluids and (viii) restricted time bracket of ~ 1.9 to 1.8 Ga during Mesoproterozoic, a period in Proterozoic times when these deposits are prolific in many fold belts of the world (Hitzman et al. 1992). The features of the IOCG deposits that are poorly constrained in the Cu-Au deposits of this region are (i) general low levels or subdued development of Fe-oxide mineralization and (ii) poor concentration of REE. Besides these, the mineralization has much less oxidized sulfide assemblages. Though mineral assemblages of most IOCG deposits imply oxidized and sulphide-poor ore fluids, more reduced pyrrhotite-bearing assemblages are not uncommon. They are reported at Eloise in the Cloncurry districts (Baker, 1998) and Ratil Condestgable (De Haller et al. 2002). The latter is being interpreted as the result of host rock influence on the invading ore-fluids (cf. Williams et al. 2005). This study has demonstrated that in Salumber-Ghatol belt the initial phase of mineralization is distinctly reduced (pyrrhotite rich) which gradually gave way to relatively more oxidized assemblages (for example development and dominance of pyrite at later stages and hematitic replacement of magnetite) development of uraninite and other hydroxides (brucite and spadaite). The Ghagri and Bhukia Cu-Au deposits possess significant concentration of magnetite pseudomorphed by hematite. At Dugocha development of magnetite is suppressed possibly due to the influence of host rock (graphite rich) assemblages. Nevertheless, significant Fe-oxide mineralization (up to 44 wt% Fe_2O_3) occurs nearer to Dugocha prospect in Matasula region where independent magnetite-rich quartzite bands constitute main litho-marker in the region. Some other occurrences like Hinglaz Mata near Bhukia has extensive development of jasperoid breccias in Fe-oxide enriched mineralized zones and feldspathic alteration halos (Ghariya et al. 2001). Therefore, in Salumber-Ghatol belt, un-economical iron-oxide mineralization occurs in significant proportion. REE, though commonly present, but is not a universal feature of all the IOCG deposits. The IOCG deposits of Chilean Andes, Mid-Atlantic, Siberian platform, Turgai in Kazakhstan, Great Bear, NW Canada are not reported to have significant REE mineralization (Barton and Johnson, 1996). We therefore argue that the Cu-Au-Fe ± U mineralization in ~1.8 Ga to 1.9 Ga old sedimentary carbonates may represent yet another type of globally distributed REE-poor IOCG type mineralization.

Nature and Source of Saline Fluids for the Cu-Au ± Fe-oxide Mineralization

The hallmark of the IOCG deposits are Na (±K ±Ca) alterations that require saline, relatively oxidized fluids to account for the presence of magnetite/hematite and sparse sulfides. The two commonly quoted and intensely argued sources include (i) magmatic-hydrothermal source and (ii) non-magmatic evaporitic source. The magmatic model requires alkali rich magmatic source that account for subordinate Fe-oxide and relatively large Na (± K) alterations. The evaporitic model requires a surface-derived or basin-derived fluids that mingles with igneous-derived solutes and flow along a large scale plumbing system and manifest in the form of extensive albitic and related alteration zones. Significant mineralogical and geochemical inhomogeneity would be expected in the non-magmatic system than in the

magmatic system. The evaporitic model explains enormous volumes of sodic alterations normally associated with this kind of deposits. Whereas both models are being discussed, the enigmatic IOCG systems continue to elude a consensus on the processes that form these deposits (Barton and Johnson, 2004).

In Salumber-Ghatol sector there are ample evidences to support ultra-saline mineralizing conditions. These include (i) regional and pervasive ultra-sodic and ultra-potassic distal and proximal alteration zones manifested in the form of a variety of feldspathic rocks with pure exsolved phases of Na- and K-feldspars; (ii) presence of scapolite, spadaite and brucite bearing assemblages; (iii) presence of high magnesian dravites at Bhukia, Dugocha and Ghagri areas with significant povondraite component and (iv) hyper-saline fluids in mineralized zones and fluids of low salinity in non-mineralized zones. The moot question, as addressed in other IOCG-type deposits (Hitzman et al. 1992; Williams et al. 2005), is whether the ultrasaline mineralizing conditions developed at these deposits are the product of fluids supplied by a non-magmatic, basin derived source or from a magmatic source. The $\delta^{18}O$ isotopic values for all the carbonate samples Salumber-Ghatol belt are much depleted compared to the much enriched values of the carbonates of evaporitic environment (Burdett et al. 1990) and in Fig.4 they plot away from the evaporitic field. In the absence of saline depositional conditions, supply of saline fluids from depositional basin to the mineralizing brines may be ruled out. The alteration zones show uniform distribution of constituent major, trace and rare-earth elements in both proximal and distal altered rocks. Such consistencies, seldom recorded in the rocks of sedimentary environments, are suggestive of a distinct magmatic lineage for the liquids responsible for the formation of altered rocks. Primitive mantle normalized multi-elemental plots for both the deposits are identical with almost identical negative troughs at Nb, Sr and positive anomalies at Nd and Th. This feature suggests common source of mineralizing fluids for all studied deposits of the belt. But the nature of the fluids for the different deposits differed distinctly. The Cu-Au ± Fe deposit of Ghagri area require ultrapotassic saline fluids to account for pervasive development of microclinites in distal zones and potassic-sodic saline fluids for the formation of albite-microcline-dolomite rocks proximal to the mineralized zones. In contrast, the distal alteration zones of Dugocha-Bhukia require ultrasodic saline fluids and the proximal alteration zones of this area require potassic-sodic saline fluids for the generation of albite-microcline rocks. Interestingly, the fluid inclusion data for quartz from granitic plutons of this region also possess fluids of very high salinity (clustering 26.03 to 10.98 wt% eq.) that suggest role of granite in contributing the saline ore-fluids (Deol et al. 2008). We therefore infer that the supply of mineralizing brines with high Na, Na+K+Mg and K-fluids in the entire Salumber-Ghatol sector through regional dilational zones is related to the second deformational event of Aravalli orogeny. The saline-influx was so intense that it created 'artificial' hypersaline-evaporitic conditions in normal depositional basin that facilitated crystallization of scapolite-brucite-spadaite bearing assemblage and povondraitic tourmalines associated with the mineralization.

Acknowledgments: This manuscript is published with the kind permission of the Deputy Director General of the Geological Survey of India, RSAS Wing, Bangalore. The authors acknowledge the help received from following officers of the Geological Survey of India during the process of data acquisition for this paper: Drs. N.C. Pant, Basab Chattopadhyay and Shyamal Sengupta (EPMA work), Dr. A.K. Dey and Dr.R.Gopal Krishna (XRF, Fluid inclusion, and XRD work), Dr. B.R. Venkatesh, Dr.S.Sarangi, and R. Hanumantha (stable isotope work), and M. Venkat Ramaiah, A Venkata Reddy, K. Jaya and G. Vijaya Babu (ICPMS work). We thank Dr. S.P. Venkata Dasu for critically going through the manuscript, and Dr. J.N. Das and Dr. R. Ananthanarayana for the encouragement and fruitful discussions. Review by anonymous reviewer has greatly improved the manuscript.

References

Ahmed, T. and Rajamani, V. (1991) Geochemistry and petrogenesis of the basal Aravalli volcanic near Nathdwara, Rajasthan. Precambrian Res., v.49, pp.327-340.

Baker, T. (1998) Alteration, mineralization and fluid evolution at the Eloise Du-Au deposit. Cloncurry district, NW Queensland. Econ. Geol., v.93, pp.50-71.

Barton, M.D. and Johnson, D.A. (1996) Evaporitic-source model for igneous-related Fe-oxide-(REE-cu-Au-U) mineralization. Geology, v.24, pp.259-262.

Barton, M.D. and Johnson, D.A. (2004) Foot prints of Fe-oxide (Cu-Au) systems. *In:* "Predictive Mineral Discovery under cover". Centre for Global Metallogeny. Spec. Publ. no.33, The University of Western Australia, pp.1-6.

Bastrakov, E.N., Skirrow, R.G. and Davidson, G.J. (2007) Fluid Evolution and origins of iron oxide Cu-Au prospects in the Olympic Dam District, Gawler Craton, South Australia. Econ. Geol., v.102, pp.1415-1440.

Basu, K.K., Chaudhuri, N.P. and Biswas, R.K. (1968), Gossanous

origin of the iron ores near Parsola, Udaipur district – a new possibility. Colloquium on exploration and development of Non-Ferrous metals in India, Lucknow, p.34.

Bejarniya, B.R. and Kirmani, I.R. (2006), Report on investigation for basemetal and associated noble metal mineralization in Ghagri Block of Salumber area, Udiapur district, Rajasthan (E-I Stage). Geol. Surv. India, Unpubl Rep., AMSE, WZ, Jaipur.

Bhattacharya, A.K., Nagrajan, K., Shekhawat, L.S. and Joshi, D.W. (1995) Stratigraphy, structure and metamorphism of the Aravalli fold belt. Rec. Geol. Surv. India, v.127(7), pp.5-9.

Bodnar, R.J. (1983) A method of calculating fluid inclusion volumes based on vapor bubble diameters and P-V-T-X properties of inclusion fluids. Econ. Geol., v.78, pp.535-542.

Brown, P.E. and Lamb, W.M. (1988) P-V-T properties of fluids in the system H_2O-CO_2-NaCl: New graphical presentation and implications for fluid inclusion studies: Geochim. Cosmochim Acta, v.53, pp.1209-1221.

Burdett, J.W., Grotzinger, J.P. and Arthur, M.A. (1990) Did major changes in the stable-isotope composition of Proterozoic sea water occur? Geology, v.18, pp.227-230.

Chawala, A.S., Srivastava, S.K., Chaturvedi, A.K. and Srivastava, P.K. (2007) Potassium Dispersion Patterns on Aero-Radiogeochemical Images, a direct indicator to hydrothermal alteration and associated mineralization – A case study from southeastern Rajasthan: National Seminar on Geochemistry, Abstracts, pp.75-77.

Cook, N.D.J. and Ashley, P.M. (1992) Metaevaporite sequence, exhalative chemical sediments and associated rocks in the Proterozoic Willyama Supergroup, south Australia: Implications of metallogenesis. Precambrian Res., v.56, pp.211-226.

De Haller, A., Zuniga, A.J., Corfu, F. and Fontbote., I. (2002) The iron-oxide-Cu-Au deposits of Raul-Condestable, Mala, Lima, Peru (abst): Congress Geol. Peruano. 11th. Abstracts, 80 p.

Deb, M. (2008) Some key issues of gold metallogeny in India: (Abstract). International. Workshop on "Gold metallogeny in India". Delhi University, pp.50-53.

Deb, M. and Thorpe, R.I. (2004) Geochronological constraints in the Precambrian Geology of Rajasthan and their metallogenic implications: *In:* M. Deb and R.I. Thorpe (Eds.), "Sediment-hosted lead-zinc sulfides with emphasis on the deposits in the northwestern Indian Shield". Narosa Publishing House, New Delhi, pp.246-263.

Deol, S., Deb, M. and Chattopadhyay (2008) Bhukia-Jagpura gold prospect, south Rajasthan: a preferred genetic model: Abst. International workshop on "Gold metallogeny in India". Delhi University, pp.119-124.

Fairchild, I.J., Marshall, J.H.D. and Bertrand-Safati, J. (1990) Stratigraphic shifts in carbon isotopes from Proterozoic stromatolitic carbonates (Mauritina): Influence of primary mineralogy and diagenesis. Amer. Jour. Sci., v.290-A, pp.46-79.

Fareeduddin, Kirmani, I.R. and Gupta, S. (2010a) Low-Al tourmalines of 'oxy-dravite'-povondraite series from Cu-Au deposit of Ghagri area, Salumber-Ghatol belt, Aravalli Supergroup, Rajasthan. Curr. Sci., v.99, pp.933-936.

Fareeduddin, Gupta, S., Golani, P.R., Kirmani, I.R. and Suresh Chander (2010b) Tourmaline as metallogenic indicator: Examples from Paleoproterozoic Pb-Zn and Cu-Au deposits of Rajasthan, India. Jour. Geol. Soc. India, v.76, pp.215-243.

Fareeduddin, Reddy, M.S. and Bose, U. (1995) Reappraisal of Delhi stratigraphy in the Ajmer-Sambhar sector, north-central Rajasthan. Jour. Geol. Soc. India, v.45, pp.667-679.

GSI (2009) GSI portal. http://www.portal.gsi.gov.in/gold

Ghariya, S.S., Jat, R.L. and Harpawat, C.L.(1998) Gold mineralization and its controls in Bhukia prospect, southeastern Rajasthan, India: *In:* M.S. Krishnan Centenary Commemorative National Seminar, v.1-2, Nov. 1998, pp.64-66.

Ghariya, S.S., Jat, R.L. and Harpavat, C.L. (2001) Hydrothermal gold mineralization in the Bhukia gold prospect of the Lower Proterozoic Aravalli Fold Belt, Rajasthan. Geol. Surv. India, Spec. Publ., no.58, pp.327-340.

Golani, P.R., Rajawat, R.S., Pant, N.C. and Rao, M.S. (1999) Mineralogy of Gold and associated Allyos in Sulfides of Bhukia Gold Prospect in Southeastern Rajasthan, Western India. Jour. Geol. Soc. India, v.64 pp.121-128.

Golani, P.R., Pandit, M.K., Sial, A.N., Fallik, A.E., Ferriera, V.P. and Roy, A.B. (2002) Ba-Na rich Paleoproterozoic Aravalli metasediments of evaporitic association, NW India: A new repository of gold mineralization. Precambrian Res., v.116, pp.183-198.

Grover, A.K. and Verma, R.G. (1993), Gold mineralization in the Precambrian (Bhukia Area) of southeastern Rajasthan – A new discovery. Jour. Geol. Soc. India, v.42, pp.281-288.

Guha, D.B. (2004) Ore petrography, mineralogy and localization of sulfide-gold mineralization of East-Central Block, Bhukia, Banswara District, Rajasthan. Geol. Surv. India, Spec. Publ., v.72, pp.175-188.

Gupta, S.N., Arora, Y.K., Mathur, R.K., Iqbaluddin., Prasad, B., Sahai, T.N. and Sharma, B. (1997) The Precambrian Geology of the Aravalli Region, Southern Rajasthan and Northwestern Gujrat: Mem. Geol. Surv. India, v.123, 262p.

Haskin, L.A., Haskin, M.A., Frey, F.A. and Wildeman, T.R., 1968, Relative abundances of rare earths. *In:* L.H. Ahrens (Ed.), Origin and distribution of elements. Pergamon, Oxford, pp.889-912.

Heron, A.M. (1953) The Geology of Central Rajputana. Mem. Geol. Surv. India, v.79, pp.1-389.

Henry, D.J., Sun, H., Slack, J.F. and Dutrow, B.L. (2008) Tourmalinites from metaevaporites and highy magnesian rocks: Perspective from Namibian tourmalinites. European Jour. Mineral., v.20, pp.889-904.

Hitzman, M.W., Oreskes, N and Eidnaudi, M. (1992) Geological Characteristics and tectonic setting of Proterozoic iron-oxide (Cu-U-Au-REE) deposits: Precambrian Res., v.58, pp.241-287.

Iqbaluddin and Bhattacharya, N.B. (1971) Systematic geological mapping in parts of Salumber belt, Udaipur district, Rajasthan.

Geol. Surv. India, Unpub. Report (FS-1969-70).

Kaufmann, A.J., Knoll, A.H., Hayes, J.M. and Awramik, S.M. (1992) Biostratigraphic and chemostratigraphic correlation of Neoproterozoic sedimentary successions: Upper Indir Group, northwestern Canada, as a test case. Geology, v.20, pp.181-185.

Kreuzer, O.P. (2005) Intrusion-hosted mineralization in the Charters Towers goldfield, North Queensland: New isotopic and fluid inclusion constraints on the timing and origin of the auriferous veins. Econ. Geol., v.100, pp.1583-1603.

Meyers, C. (1988) Ore deposits as guides to geologic history of the earth. Ann Rev. Earth Planet. Sci., v.16, pp.147-171.

Naha, K. and Halyburton, R.V. (1974) Early Precambrian stratigraphy of Central and Southern Rajasthan, India. Precambrian Res., v.1, pp.55-73.

Nielsen, H. (1979) Sulfur Isotopes. *In:* E. Joger and J.C. Hunzikov (Eds.), Lectures in Isotope Geology. Springer Verlaag, Berlin, Hiedelberg, pp.283-312.

Oliver, N.H.S., Cleverlay, J.S., Mark, G., Pollard, P.J., Bin-Fu, Marshal, L.J., Rubenach, M.J., Williams, P.J. and Baker, T. (2004) Modeling the role of sodic alteration in the genesis of Iron-oxide-Copper-Gold Deposits, Eastern Mount Isua Block, Australia. Econ. Geol., v.99, pp.1145-1176.

Oreskes, N. and Eidnaudi, M.T. (1990) Origin of REE-enriched hematite breccias at Olympic Dam Cu-Au-U-Au-Ag deposits, Roxby Downs, South Australia. Econ. Geol., v.85, pp.1-28.

Oreskes, N. and Eidnaudi, M.T. (1992) Origin of hydrothermal fluids of Olympic Dam: Preliminary results from fluid inclusion and stable isotopes. Econ. Geol., v.87, pp.64-90.

Rao, M.S., Fareeduddin, Godhavari, K.S., Suresh Chander and Sisodia,C.P. (2004) Carbonaceous Metaexhalite of Shungitic Affinity in Palaeoproterozoic Aravalli Supergroup, Dugocha Area, Rajasthan. Jour. Geol. Soc. India, v.63, pp.522-532.

Roedder, E. (1984) Fluid Inclusions: Reviews in Mineralogy, v.12, Min. Soc. Am., 644p.

Roy, A.B. (1988) Stratigraphic and tectonic framework of the Aravalli Mountain Range. *In:* A.B. Roy (Ed.), Precambrian of Aravalli Mountain Range, Rajasthan, India. Mem., Geol. Soc. India, no.7, pp.3-31.

Sharma, R.S. (1988) Patterns of metamorphism in the Precambrian rocks of the Aravalli Mountain Belt. *In:* A.B. Roy (Ed.), Precambrian of Aravalli Mountain Range, Rajasthan, India. Mem. Geol. Soc. India, no.7, pp.33-76.

Shepherd, T.J., Rankin, A.H and Alderton, D.H.M. (1985) A practical guide to fluid inclusion studies. Blackie and Sons, 238p.

Shields, G. and Veizer, J. (2002) Precambrian marine carbonate isotope database: version 1.1, Geochemistry, Geophysics, Geosystems. v.3, No.6. 10.1029/2001GC000266.

Singh Govind., Singh, Rajendra., Sharma D.K., Yadav O.P. and Jain, Rajan B. (2007) Uranium and REE potential of the albitite-pyroxenite-microclinite belt of Rajasthan, India: (Abstract) National Seminar on Geochemistry, Hyderabad, India.

Sinha-Roy, S. (1988) Proterozoic Wilson cycles in Rajasthan. *In:* A.B. Roy (Ed.), Precambrian of Aravalli Mountain Range, Rajasthan, India. Mem. Geol. Soc. India, v.7, pp.95-109.

Skirrow, R.G and Davidson,G.J. (2007), 'Preface' – 'A Special issue devoted to Proterozoic Iron Oxide Cu-Au-(U) and gold mineral systems of the Gawler Craton. Econ. Geol., v.102, pp.1373-1376.

Sreenivas, B., Das Sharma, S., Kumar B., Patil, D.J., Roy, A.B and Srinivasan, R. (2001) Positive $\delta^{13}C$ excursion in carbonate and organic fractions from the Paleoproterozoic Aravalli Supergroup, Northwestern India. Precambrian Res., v.106, pp.277-290.

Sun, S.S. and McDonough, W.F. (1989) Chemical and isotopic systematic of ocean basalts: implications for mantle composition and processes. *In:* A.D. Saunders and M.J. Norry (Eds.), "Magmatism in Ocean Basins, Blackwell Scientific Publications, pp.313-346.

Suresh Chander and Sisodia, C.P. (2003) Gold mineralization in the Paleoproterozoic rocks of Sanjela-Manpur-Dugocha Belt, Salumber Area, Udaipur district, Rajasthan. Jour. Geol. Soc. India, v.61, pp.463-470.

Williams, P.J., Barton, M.D., Johnson, D.A., Fontrote,L., De Haller, A., Mark,G. and Oliver, N.H.S. (2005) Iron oxide Copper-Gold Deposits; Geology, Space-Time Distribution and possible modes of origin. Econ. Geol., 100th Anniversary Volume, pp.371-405.

Zhang, Y.G and Frantz, J.D. (1987) Determination of the homogenization temperatures and densities of superficial fluids in the system NaCl-KCl-$CaCl_2$-H_2O using synthetic fluids inclusions. Chem. Geol., v.64, pp.335-350.

(Received: 21 December 2010; Revised form accepted: 7 April 2011)